

THE INITIAL-FINAL MASS RELATION: DIRECT CONSTRAINTS AT THE LOW-MASS END^{1,2}

JASONJOT S. KALIRAI,^{3,4} BRAD M. S. HANSEN,⁵ DANIEL D. KELSON,⁶ DAVID B. REITZEL,⁵
R. MICHAEL RICH,⁵ AND HARVEY B. RICHER⁷

Received 2007 June 29; accepted 2007 November 15

ABSTRACT

The initial-final mass relation represents a mapping between the mass of a white dwarf remnant and the mass that the hydrogen-burning main-sequence star that created it once had. The empirical relation thus far has been constrained using a sample of ~ 40 stars in young open clusters, ranging in initial mass from ~ 2.75 to $7 M_{\odot}$, and shows a general trend that connects higher mass main-sequence stars with higher mass white dwarfs. In this paper, we present CFHT CFH12K photometric and Keck LRIS multiobject spectroscopic observations of a sample of 22 white dwarfs in two *older* open clusters, NGC 7789 ($t = 1.4$ Gyr) and NGC 6819 ($t = 2.5$ Gyr). We measure masses for the highest signal-to-noise ratio spectra by fitting the Balmer lines to atmosphere models and place the first direct constraints on the low-mass end of the initial-final mass relation. Our results indicate that the observed general trend at higher masses continues down to low masses, with $M_{\text{initial}} = 1.6 M_{\odot}$ main-sequence stars forming $M_{\text{final}} = 0.54 M_{\odot}$ white dwarfs. When added to our new data from the very old cluster NGC 6791, the relation is extended down to $M_{\text{initial}} = 1.16 M_{\odot}$ (corresponding to $M_{\text{final}} = 0.53 M_{\odot}$). This extension of the relation represents a fourfold increase in the total number of hydrogen-burning stars for which the integrated mass loss can now be calculated from empirical data, assuming a Salpeter initial mass function. The new leverage at the low-mass end is used to derive a purely empirical initial-final mass relation. The sample of white dwarfs in these clusters also shows several interesting systems that we discuss further: a DB (helium) white dwarf, a magnetic white dwarf, a DAB (mixed hydrogen/helium atmosphere or a double degenerate DA+DB) white dwarf(s), and two possible equal-mass DA double degenerate binary systems.

Subject headings: open clusters and associations: individual (NGC 6819, NGC 7789) — stars: evolution — techniques: photometric — techniques: spectroscopic — white dwarfs

Online material: color figures

1. INTRODUCTION

The initial-final mass relation denotes a mapping from the initial mass of a main-sequence star to its final white dwarf configuration and hence provides the total mass loss that a star has undergone through its lifetime, a fundamental property of stellar evolution (Reimers 1975; Renzini & Fusi Pecci 1988; Weidemann 2000). At one extreme, a small extrapolation of the high-mass end of the relation can lead to constraints on the critical mass that separates white dwarf production from Type II supernova explosions. This can therefore be used to estimate energetics involved in feedback processes through the prediction of the birth rates of Type II supernovae and neutron stars (van den Bergh & Tammann 1991). At the opposite extreme, the relation represents a rare tool to probe the progenitor properties of the majority of the evolved

stars in old stellar populations (most of which are now low-mass white dwarfs). If constrained over a large mass range (i.e., $1-7 M_{\odot}$), the relation can be a powerful input to chemical evolution models of galaxies (including enrichment in the interstellar medium) and therefore enhances our understanding of star formation efficiencies in these systems (Somerville & Primack 1999).

The importance of the initial-final mass relation has been recently compounded as a result of the discovery of thousands of white dwarfs in both the Galactic disk and halo. For the former, the Sloan Digital Sky Survey has spectroscopically confirmed many new white dwarfs, bringing the total number of such objects in our Galaxy to almost 10,000 (Eisenstein et al. 2006). This has led to an improved white luminosity function for the disk of our Galaxy that shows an abrupt truncation at $M_{\text{bol}} = 15.3$ (Harris et al. 2006). In the Galactic halo, recent *Hubble Space Telescope* (*HST*) observations of the globular clusters M4 (Richer et al. 2004; Hansen et al. 2004), Omega Cen (Monelli et al. 2005), and NGC 6397 (Richer et al. 2006; Hansen et al. 2007) have similarly uncovered several thousand cluster white dwarfs. Modeling the luminosity functions of the disk white dwarfs and the cooling sequences of the halo star clusters, directly yields the ages of the Galactic disk and halo components. In both cases, the white dwarf samples are dominated by low-mass stars, and therefore such modeling requires an input initial-final mass relation that is well understood at the low-mass end (e.g., Ferrario et al. 2005; Hansen et al. 2007).

The first attempt to derive an initial-final mass relation was made by Weidemann (1977). He compared theoretical models of mass loss (e.g., Fusi-Peccci & Renzini 1976) to the observed masses of a few white dwarfs in the nearby Hyades and Pleiades, and concluded that the observed mass loss was larger than model predictions. Shortly after this pioneering work, Romanishin &

¹ Data presented herein were obtained at the W. M. Keck Observatory, which is operated as a scientific partnership among the California Institute of Technology, the University of California, and the National Aeronautics and Space Administration. The Observatory was made possible by the generous financial support of the W. M. Keck Foundation.

² Based on observations obtained at the Canada-France-Hawaii Telescope (CFHT), which is operated by the National Research Council of Canada, the Institut National des Sciences de l'Univers of the Centre National de la Recherche Scientifique of France, and the University of Hawaii.

³ University of California Observatories, Lick Observatory, University of California, Santa Cruz, CA 95060; jkalirai@ucolick.org.

⁴ Hubble Fellow.

⁵ Department of Physics and Astronomy, Box 951547, Knudsen Hall, University of California, Los Angeles, CA 90095; hansen@astro.ucla.edu, reitzel@astro.ucla.edu, rmr@astro.ucla.edu.

⁶ Carnegie Observatories, Carnegie Institution of Washington, 813 Santa Barbara Street, Pasadena, CA 91101; kelson@ociw.edu.

⁷ Department of Physics and Astronomy, University of British Columbia, Vancouver, BC V6T 1Z1, Canada; richer@astro.ubc.ca.

Angel (1980) and Anthony-Twarog (1981, 1982) used photographic plates to search for new white dwarf candidates in several young open clusters, including NGC 1039, NGC 2168, NGC 2287, NGC 2422, NGC 2632 (Praesepe), NGC 6633, NGC 6405, and IC 2602. These studies modeled the expected numbers of white dwarfs in each cluster and estimated limits on the boundaries for the upper progenitor mass limit to white dwarf production ($5-7 M_{\odot}$). Solid constraints on the relation came from subsequent spectroscopic observations of these white dwarfs as well as newly discovered degenerate stars in nearby open clusters (Koester & Reimers 1981, 1985, 1993, 1996; Reimers & Koester 1982, 1989, 1994; Weidemann & Koester 1983; Weidemann 1987, 1997; Jeffries 1997). The result of this enormous two-decade-long effort was an initial-final mass relation consisting of ~ 20 data points, from observations of roughly a half-dozen open star clusters (see Weidemann [2000] for a review). The final relation shows a clear trend with higher mass main-sequence stars producing increasingly more massive white dwarfs.

In the last few years, the amount of data constraining the initial-final mass relation has more than doubled (Claver et al. 2001; Dobbie et al. 2004, 2006; Williams et al. 2004; Kalirai et al. 2005b; Liebert et al. 2005b; Williams & Bolte 2007). Although the general trend of the relation remains intact, the scatter has increased, possibly signifying a relation between the stellar mass loss and the properties of the host environment (e.g., metallicity effects; Kalirai et al. 2005b). As an extreme example, the recent study of the white dwarf population of the supersolar metallicity star cluster NGC 6791 ($[Fe/H] = +0.4$) has revealed it to be significantly undermassive relative to the field distribution. This is clear evidence that the progenitor stars of these remnants experienced enhanced mass loss in post-main-sequence evolutionary stages due to the high metallicity of the cluster (Kalirai et al. 2007).

Prior to this study, the oldest open star clusters that have been successfully targeted for white dwarf spectroscopy to build an initial-final mass relation were the Hyades and Praesepe.⁸ The ages of both of these systems are 600–700 Myr (Perryman et al. 1998; Claver et al. 2001), indicating that the present-day turnoff masses are $\gtrsim 2.75 M_{\odot}$. This threshold therefore represents the current low-mass anchor on the initial-final mass relation, as all of the white dwarfs in these clusters must have evolved from main-sequence progenitors with a mass larger than $\sim 2.75 M_{\odot}$. A very small fraction of all stars in the universe have masses this large, and therefore the relation is often extrapolated to lower masses to provide useful input. Spectroscopic white dwarf studies have been unable to target any old open clusters ($t > 1$ Gyr) for several reasons. Primarily, few photometric studies exist that have identified populations of white dwarf candidates in these clusters. Second, the known rich old open clusters are generally much farther (>10 times) than nearby clusters such as the Hyades and Praesepe. Finally, because of their older age, most cluster white dwarfs in these systems have cooled to very faint magnitudes, thus making it difficult to obtain high-quality spectra of the stars.

White dwarfs in the nearest globular star clusters have also recently been targeted for mass measurements by several groups. The only successful campaign measured a mean mass of $0.53 M_{\odot}$ for white dwarfs in NGC 6752 (Moehler et al. 2004). Given the lower signal-to-noise ratio (S/N) of these data, the temperature of the stars was measured from the spectra and then combined with photometric information to yield a mass. This mean mass is consistent with several independent arguments that all suggest

the masses of white dwarfs in globular clusters should be $0.51-0.55 M_{\odot}$ (Renzini & Fusi Pecci 1988; Renzini et al. 1996).

The combination of large mosaic cameras on 4 m telescopes (e.g., CFH12K MegaCam on the Canada-France-Hawaii Telescope) and the advent of blue-sensitive multiobject spectrographs on 10 m telescopes (e.g., the Low Resolution Imaging Spectrograph [LRIS] on Keck; Oke et al. 1995) provide the resources necessary to extend the study of the initial-final mass relation to a new regime. In this paper we present direct spectroscopic mass determinations of white dwarfs in open clusters older than 1 Gyr. The very rich clusters NGC 7789 and NGC 6819 are ~ 2 and ~ 4 times older than the Hyades/Praesepe systems, respectively, and have been recently studied by our team using the Canada-France-Hawaii Telescope to very faint magnitudes ($V \sim 25$). The data have uncovered hundreds of white dwarf candidates, a subset of which have been followed up with the Keck 10 m telescope and LRIS multiobject spectrograph. In § 2 we present our photometric observations of NGC 7789 and NGC 6819 and construct the deepest color-magnitude diagrams (CMDs) for each cluster to date (§ 3). Parameters (e.g., distance, reddening, and age) are derived for each cluster. In § 4 we discuss the construction of multiobject spectroscopic masks to observe the candidate white dwarfs in each cluster and describe the general spectroscopic observations. This includes the selection of white dwarf candidates from the imaging catalogs. The spectra for all confirmed DA (hydrogen atmosphere) white dwarfs are presented in § 5 and fit to synthetic spectra to derive T_{eff} , $\log g$, masses, and cooling ages in § 6. We eliminate field white dwarfs from our sample and calculate the progenitor masses for each of the cluster white dwarfs in § 7. This is used to build a new empirical initial-final mass relation extending down to $M_{\text{initial}} = 1.6 M_{\odot}$. When added to our recent study of the 8.5 Gyr cluster NGC 6791, the relation is now mapped down to $M_{\text{initial}} = 1.16 M_{\odot}$. The results are presented and analyzed in § 8, and the study is summarized in § 9.

2. CFHT PHOTOMETRY

All of the imaging observations of NGC 7789 and NGC 6819 were obtained with the CFH12K mosaic CCD camera on the 4 m Canada-France-Hawaii Telescope (CFHT), as a part of the CFHT Open Star Cluster Survey (Kalirai et al. 2001b). The camera contains 12 CCDs, each with 2048×4096 pixels (a total of over 100 million pixels), at an individual pixel scale of $0.206''$. The projection on the sky is $42' \times 28'$, and therefore the dominant population of both clusters is probed out to near the tidal radii.

We imaged NGC 7789 from 2001 late May to mid-July in the V and B filters. Similarly, NGC 6819 data were acquired in the same filters in 1999 October, 2001 April, and 2001 August. Multiple deep exposures were taken to achieve a solid detection of the white dwarf cooling sequence in each cluster (no previous white dwarfs had been found in either system). Shallower exposures were also obtained to fill in the brighter main-sequence, turnoff, and giant stars, which are saturated on the longer frames. In all exposures, the clusters were placed near the center of the mosaic camera to allow a suitable blank field to be constructed from the outer CCDs.

The observing conditions were very good for the majority of the exposures (photometric skies, subarcsecond seeing conditions, and low air masses). A log of the data used in the final analysis is presented in Table 1.

The data reduction for NGC 6819 is described in detail in Kalirai et al. (2001c). The final photometric and astrometric catalogs used in the present study are identical to that earlier set. For NGC 7789, we processed the science frames according to the prescription in Kalirai et al. (2001b). Summarizing, we obtained several flat-field, bias, and dark images and applied these to the

⁸ Fleming et al. (1997) also discuss one object along M67's sight line whose membership remains uncertain.

TABLE 1
OBSERVATIONAL LOG OF IMAGING DATA

Filter	Exposure Time (s)	Number of Images	Air Mass
NGC 7789			
<i>V</i>	600	14	1.25–1.43
<i>V</i>	90	1	1.67
<i>V</i>	10	1	1.25
<i>V</i>	5	1	1.28
<i>V</i>	1	1	1.73
<i>V</i>	0.5	1	1.69
<i>B</i>	800	12	1.25–1.42
<i>B</i>	120	1	1.35
<i>B</i>	10	1	1.36
<i>B</i>	1	1	1.37
<i>B</i>	0.5	1	1.37
NGC 6819			
<i>V</i>	300	9	1.16–1.31
<i>V</i>	50	1	1.16
<i>V</i>	10	1	1.15
<i>V</i>	1	1	1.27
<i>B</i>	300	9	1.40–1.76
<i>B</i>	50	1	1.38
<i>B</i>	10	1	1.37
<i>B</i>	1	1	1.25

individual science frames using the FITS Large Images Processing Software⁹ (FLIPS; see also Kalirai et al. 2001b). FLIPS was next used to register and co-add the multiple science exposures for a given exposure time (which were each dithered slightly). Photometry was performed on the resulting images using a variable point-spread function in DAOPHOT (Stetson 1994), and calibrated using Landolt standard star field observations (Landolt 1992), as discussed in §§ 5.1 and 5.2 of Kalirai et al. (2001b). The final errors in the photometry are very well behaved. We find $\sigma_V < 0.05$ mag down to $V = 24$ and $\sigma_V < 0.10$ mag down to $V = 25$.

3. COLOR-MAGNITUDE DIAGRAMS

NGC 7789 and NGC 6819 are two of the richest open star clusters in the Milky Way. As we show below, the clusters are both old and located at a similar distance from the Sun. The positions of these systems in the Galaxy are also quite similar; they are both found within 10° of the plane of the Galactic disk at $l = 115.5^\circ$ (NGC 7789) and $l = 74.0^\circ$ (NGC 6819). Not surprisingly, the CMDs of the two clusters are strikingly similar, as shown in Figure 1. The contrast of the cluster main sequences over the foreground and background Milky Way disk and halo populations is very strong. In the observational plane, the main sequence can be seen extending from the bluest point on the present-day turnoff ($V \sim 14.6$ and $B - V \sim 0.6$ for NGC 7789; $V \sim 15.4$ and $B - V \sim 0.6$ for NGC 6819) down to the photometric limit. Just to the red of the main sequence, an equal-mass binary sequence can be seen in NGC 6819 and also possibly in NGC 7789. As we showed through synthetic CMD fitting in Kalirai

⁹ See <http://www.cfht.hawaii.edu/~jcc/Flips/flips.html>.

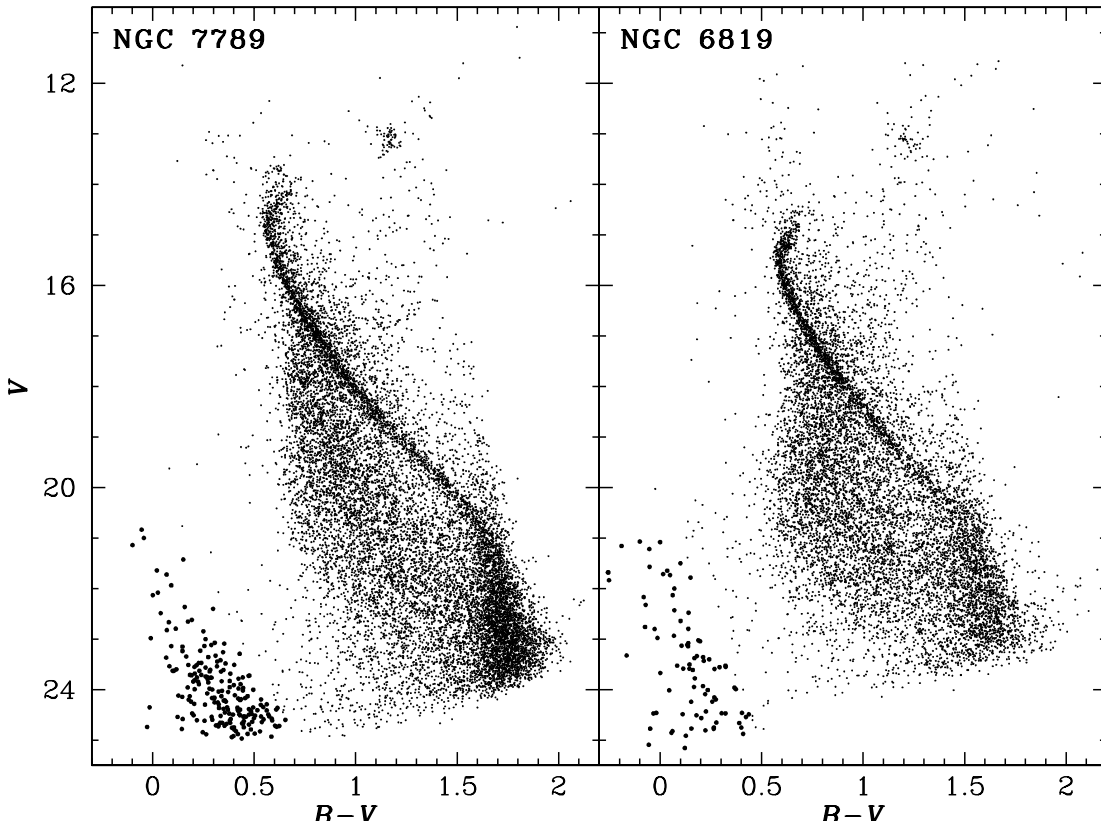


FIG. 1.—CMDs of NGC 7789 and NGC 6819, showing very tight main sequences, turnoffs, and post-main-sequence evolutionary phases. For example, a “hook” is seen above the turnoff, designating the contraction of stars that have just exhausted their hydrogen supply. These are the deepest CMDs constructed for these clusters to date, and the faint blue region of the CMDs reveals a large population of white dwarfs in each cluster (see also Kalirai et al. 2001c).

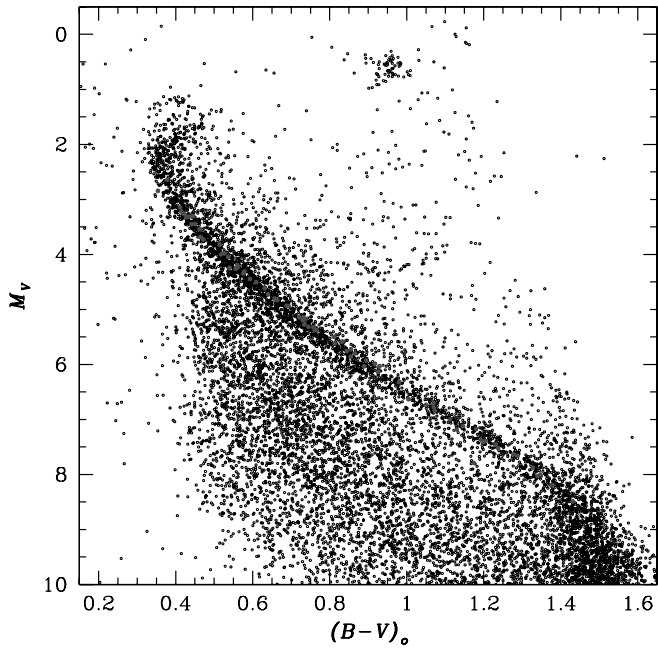


Fig. 2.—Distance modulus of NGC 7789, measured to be $(m - M)_V = 12.5 \pm 0.1$ by matching the observed cluster main sequence (blue edge) to the Hyades (gray dots). The slope of the two main sequences are in excellent agreement over the entire CMD. In this plane, all adjustments (distance, reddening, and color offset due to metallicity difference) have been made to the NGC 7789 stars (see § 3.1). [See the electronic edition of the Journal for a color version of this figure.]

& Tosi (2004) the fraction of binary stars in NGC 6819 is $\sim 20\%-30\%$. The turnoff of both clusters is clearly defined, as well as an apparent “hook” just above the brightest point. This hook is caused by a small contraction of the stellar core just above the turnoff. Few, if any, stars are seen in the subgiant branch given the shorter evolutionary timescale of this phase of post-main-sequence evolution. However, several blue straggler candidates are found above the turnoff in both clusters, especially in NGC 6819. The horizontal branches are manifested as red clumps, as expected given the higher metallicity of stars in these two systems. Evolution off the red giant clump is also seen at the bright red part of the CMDs.

These CMDs of NGC 7789 and NGC 6819 are the deepest ever constructed for the clusters (note: NGC 6819 was presented in Kalirai et al. 2001c). As expected, each CMD shows a large population of white dwarfs that had previously not been detected. These cooling sequences, in the faint blue part of the diagrams, extend several magnitudes to the limit of the data (these points have been made larger for clarity). Unlike our study of the 0.5 Gyr cluster NGC 2099 (Kalirai et al. 2001a), these two clusters are old enough that the coolest white dwarfs ($V = 26-27$) are beyond our detection limit. The scatter in the cooling sequences results from a combination of photometric errors and field contamination, which we will address later in § 7.1.

3.1. Distance and Age Measurements

With just two-color photometry, it is very difficult to simultaneously constrain the reddening and distance of a star cluster. When fitting the main sequence, these parameters are degenerate. Fortunately, the reddening can be measured independently from multifilter photometry. Wu et al. (2007) recently presented a 13-color CCD spectrophotometric study of NGC 7789 and conclude with an estimate of the foreground reddening to NGC 7789 of $E(B - V) = 0.28 \pm 0.02$. In their Table 1, they also list previous measurements (dating back to the work of Burbidge & Sandage 1958) and find that their value is in fact nicely

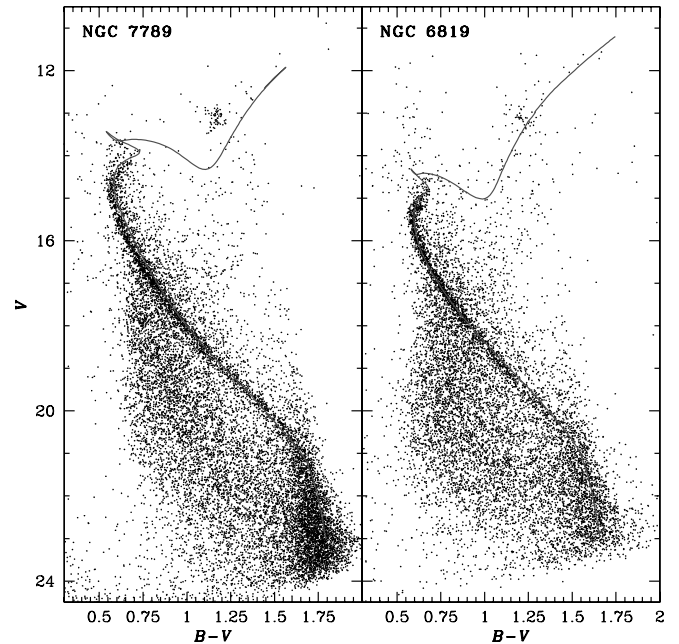


Fig. 3.—Stellar isochrones from VandenBerg et al. (2006), found to be in excellent agreement with the main sequence and main-sequence turnoff of NGC 7789 and NGC 6819 (although there is a disagreement on the red giant branch of NGC 7789). As summarized in § 3.1, we measure an age of $t = 1.4$ Gyr for NGC 7789 and $t = 2.5$ Gyr for NGC 6819. [See the electronic edition of the Journal for a color version of this figure.]

bracketed by the findings in these independent studies [$0.22 < E(B - V) < 0.35$; see references within Wu et al. 2007].

The cornerstone technique of determining the distance of an open star cluster involves fitting the observed main sequence to that of the Hyades. As one of the nearest star clusters to the Sun ($d = 46.34 \pm 0.27$ pc; Perryman et al. 1998), the distance to each of the Hyades main-sequence stars is accurately known through parallax measurements (to within $\sim 2\%$; de Bruijne et al. 2001). Therefore, one can directly overlay the Hyades main-sequence stars [in an M_V , $(B - V)_0$ plane] to the observed cluster main sequence and adjust the distance modulus of the latter until the two overlap. Although NGC 7789 is much older than the Hyades (more than a factor of 2), our deep photometry presents a long, unevolved main sequence for this comparison. We do, however, need to make a slight adjustment given the different metallicities of the clusters. The Hyades is slightly more metal-rich than the Sun, $Z = 0.024$ (Perryman et al. 1998), whereas NGC 7789 is slightly more metal-poor, $Z = 0.014$ (average of recent literature values; see Wu et al. 2007). Correcting this offset amounts to a very small color shift of the main sequence. The resulting comparison yields an excellent alignment of the two main sequences for an NGC 7789 distance modulus of $(m - M)_V = 12.5 \pm 0.1$, where the error bar is derived as described in § 8.4 of Kalirai et al. (2001a). This is illustrated in Figure 2, where we have overlaid the Hyades stars on top of the shifted NGC 7789 main sequence.

Using a similar analysis, Kalirai et al. (2001c) determined the reddening and distance modulus of NGC 6819 to be $E(B - V) \sim 0.10-0.14$ (see also Bragaglia et al. 2001) and $(m - M)_V = 12.30 \pm 0.12$.

With an estimate of the fundamental parameters in place, we can measure the ages of both clusters using our derived CMDs. For this, we have chosen to use the stellar isochrones from VandenBerg et al. (2006), which include a more physical treatment of convective overshooting than past generation models (see below for a comparison with other models). Our results are shown in Figure 3.

Assuming $[\alpha/\text{Fe}] = 0$, our CMD for NGC 7789 favors an isochrone with $t = 1.4$ Gyr. The resulting fit to the entire main sequence and turnoff is good, although the cluster red giants are bluer than the model prediction. We note that VandenBerg et al. (2006) also found this discrepancy when fitting an older photometric data set (V, I) of this cluster (observed by Gim et al. 1998). The cause of this mismatch may be in part related to the masses of these red giant stars, which, given the age of NGC 7789, should be very close to the phase transition threshold where the evolution is terminated by degenerate helium ignition in the core (i.e., the flash). Modeling this transition depends sensitively on the extent of core overshooting. For NGC 6819, we find that an isochrone of age $t = 2.5$ Gyr reproduces all of the main CMD features very nicely. This includes the main sequence, turnoff, and red giant branch. For both clusters, the ages determined from the VandenBerg et al. (2006) isochrones are consistent at the $\sim 10\%$ level with those determined from either the Yale-Yonsei isochrones (Demarque et al. 2004) or the Padova group isochrones (Girardi et al. 2002).

To summarize the analysis of the cluster CMDs, our best parameters are $E(B - V) = 0.28 \pm 0.02$, $(m - M)_V = 12.5 \pm 0.1$, $Z = 0.014$, and $t = 1.4$ Gyr for NGC 7789. For NGC 6819, we find $E(B - V) = 0.13 \pm 0.02$, $(m - M)_V = 12.30 \pm 0.12$, $Z = 0.017$, and $t = 2.5$ Gyr. We point out that these age derivations are sensitive to the input parameters. A reasonable fit to the observed CMDs can be achieved by tweaking the age by $\sim 10\%$ with corresponding changes to the reddening, distance moduli, and/or metallicity. Although we cannot be absolutely certain which combination of these parameters are correct for the clusters (given the ranges reported in the literature), we are reasonably sure that our estimates are accurate, as they agree with most recent literature values. It is also reassuring that, for this set of parameters, the models reproduce the lower main sequences nearly perfectly (this phase has never been tested before).

4. KECK SPECTROSCOPY

Spectroscopic observations of NGC 7789 and NGC 6819 were obtained using the LRIS multiobject spectrograph on the Keck I telescope on 2005 July 29 and 30 (each cluster was observed for approximately half the night, on both nights). The instrument is a dual-beam, low-resolution spectrograph with a $5' \times 7'$ field of view (Oke et al. 1995; McCarthy et al. 1998). For the blue side, we used the 600/4000 grism (dispersion = $0.63 \text{ \AA pixel}^{-1}$), which simultaneously covers 2580 \AA , from 3300 to 5880 \AA . The plate scale of the blue CCD is $0.135 \text{ arcsec pixel}^{-1}$. For the red side, we used the 600/7500 grating (dispersion = $1.28 \text{ \AA pixel}^{-1}$), centered at 6600 \AA , which covers a wavelength baseline of 2620 \AA . The plate scale of the red CCD is $0.210 \text{ arcsec pixel}^{-1}$. The light to the blue side was intercepted from the collimator mirror using the D560 dichroic. In multiobject slit spectroscopy, the exact wavelength coverage for each target varies somewhat depending on the location of that target on the mask.

We do not a priori know *which* of the faint blue stars identified as white dwarf candidates from the imaging observations are in fact white dwarfs. Unresolved background galaxies, QSOs, hot subdwarfs, and even distant early-type main-sequence stars can contaminate the sample. However, NGC 7789 and NGC 6819 are two of the richest Milky Way open star clusters, and therefore the percentage of contaminating field objects is suppressed. In fact, Figure 1 shows that both clusters exhibit obvious white dwarf cooling sequences which would not be otherwise discernible if field contamination was overwhelming. We also note that similar studies by our group of the rich cluster NGC 2099 (Kalirai et al. 2005b) and NGC 6791 (Kalirai et al. 2007) have confirmed that

most faint blue objects in our CFHT CMDs for these rich systems are in fact cluster white dwarf members.

We generate an input list of spectroscopic targets by assigning priorities to objects in the CFHT CMD based on their magnitudes and morphology (i.e., clearly extended sources with a stellarity index < 0.25 are removed; Bertin & Arnouts 1996). Objects that are near the bright white dwarf cooling sequence (defined by eye; see Fig. 1) in each cluster are given high priorities, and objects that are fainter are given lower priorities. Since the LRIS field of view is much smaller than our wide-field CFHT image, we strategically position the spectroscopic mask to overlap as many of the best targets as we can. Our expectation was to observe a single field in each of the clusters to maximize the S/N of the resulting spectra, which is critical to derive accurate masses (see § 6). However, we generated spectroscopic masks at two different locations in case a quick reduction of the data from the first exposure taken at the telescope revealed that most of the targets were not white dwarfs. In this case, we had the option to abandon further exposures of that particular field and switch to the second mask, which targeted a different region of the cluster.

For each mask location discussed above (and similarly two locations in NGC 6819), we milled two masks with individual slit widths of $0.8''$ and $1.0''$, and orientations close to the parallactic angle. The choice between the two masks was made dependent on the seeing conditions of the observations. The individual exposure times were set to 30–60 minutes for a total integration of 6.8 hr on NGC 7789 (one exposure was cut short) and 5 hr on NGC 6819. The air mass of the observations ranged from 1.25 to 1.49 for the NGC 7789 spectra and from 1.07 to 1.22 for the NGC 6819 spectra. For both clusters, the second priority mask was not observed, as a quick reduction of the data after the first exposure indicated that most of the targets were in fact DA white dwarfs (e.g., broad Balmer lines seen in the spectra). In total, the NGC 7789 spectroscopic field contained 15 targets, 9 of which were top-priority white dwarf candidates. For NGC 6819, 13 objects were targeted in the one mask, of which 8 were top-priority candidate white dwarfs. Additional box slits were used for alignment. The locations of these 28 selected white dwarf candidates on the faint blue corners of the cluster CMDs are displayed in Figure 4, for each of NGC 7789 and NGC 6819. We have also introduced a numbering scheme to identify these objects later (i.e., object “1” in NGC 7789 is labeled as NGC 7789-1). The selected objects sample the observed white dwarf cooling sequence over approximately 3 mag, in each cluster. The solid curve represents a $0.6 M_{\odot}$ white dwarf cooling sequence (Wood 1995). Postage-stamp cutouts of each of the 28 white dwarf candidates from the CFHT imaging are shown in Figure 5, and the photometric properties of these stars are summarized in Table 2.

The spectroscopic data were analyzed as described in Kalirai et al. (2007). Specifically, we used Python routines that are described in Kelson et al. (2000) and Kelson (2003) to perform bias subtraction, vertical distortion corrections, wavelength calibration (typical rms scatter in the dispersion solutions is $< 0.05 \text{ \AA}$), flat-field corrections, and sky subtraction. Standard IRAF tasks were used to extract these to one-dimensional spectra, co-add individual exposures, and flux calibrate using a spectrophotometric standard star (HZ 44). Of the 28 objects targeted on the two masks, we recovered a spectrum for all but one. This one faint object (NGC 7789-13) has $V = 23.47$ and $B - V = 0.24$ and was given a very short slit length, as its position was between two other high-priority stars. The multiobject data reduction for this slit failed at several steps of the pipeline (e.g., wavelength calibration and sky subtraction) in each of the individual exposures despite several attempts to recover a reduced spectrum.

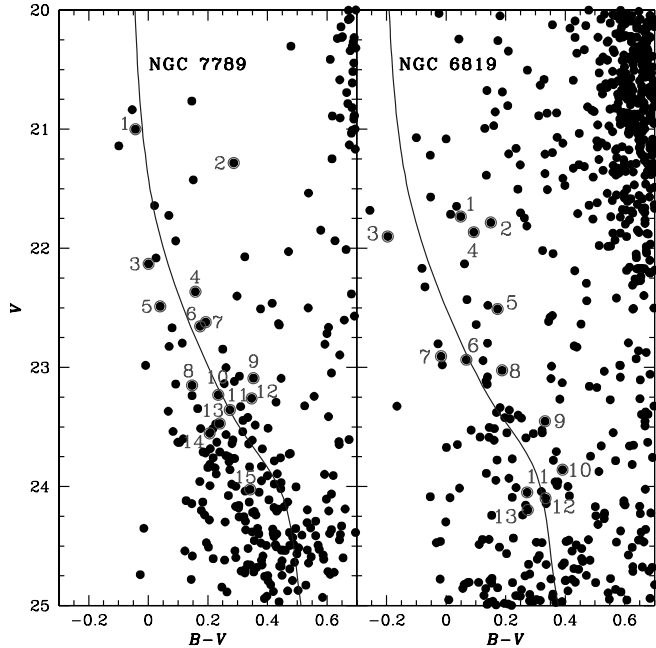


FIG. 4.—The 28 white dwarf candidates that are spectroscopically targeted in NGC 7789 and NGC 6819, highlighted in the faint blue corner of the cluster CMDs. These objects are scattered around a $0.6 M_{\odot}$ cooling sequence (Wood 1995) and span approximately 3 mag of the white dwarf cooling sequence in each cluster. [See the electronic edition of the Journal for a color version of this figure.]

5. NGC 7789 AND NGC 6819 WHITE DWARF SPECTRA

The spectra for the 27 extracted white dwarf candidates targeted in this study are shown in Figures 6 and 7. The majority of the 27 targets show clear evidence for pressure-broadened Balmer lines and are therefore DA (hydrogen atmosphere) white dwarfs. The top group of 10 white dwarfs in Figure 6 represent our highest quality data, and will be used in the analysis that follows. These stars are clearly among the brightest in our data set, and all have $S/N = 30–130$ per resolution element (measured at $\sim 4200 \text{ \AA}$) and exhibit well-defined Balmer lines from $H\beta$ down to $H8$ and $H9$. We discuss these objects further in § 6.

5.1. Rare White Dwarfs

The second set of targets in Figure 6 (bottom) represent three rare objects in our sample. Each of these stars is potentially very important (for different reasons), and so we discuss them in turn. The first, object 4 in NGC 6819, is clearly a DB (helium atmosphere) white dwarf. He absorption lines at 3889, 4471, and 4713 Å are all seen in the stellar spectrum (see three panels on the right in Fig. 6 for a closer look at these features). If a member of the cluster, this star therefore represents one of only four helium atmosphere white dwarfs found in all open clusters. The other such stars are the DBA white dwarf LP 475-242 in the Hyades, the DQ white dwarf NGC 2168:LAWDS 28 in NGC 2168 (Williams et al. 2006), and the newly discovered DB white dwarf NGC 6633:LAWDS 16 in NGC 6633 (Williams & Bolte 2007). Unfortunately, the spectral quality of NGC 6819-4 is too low to estimate

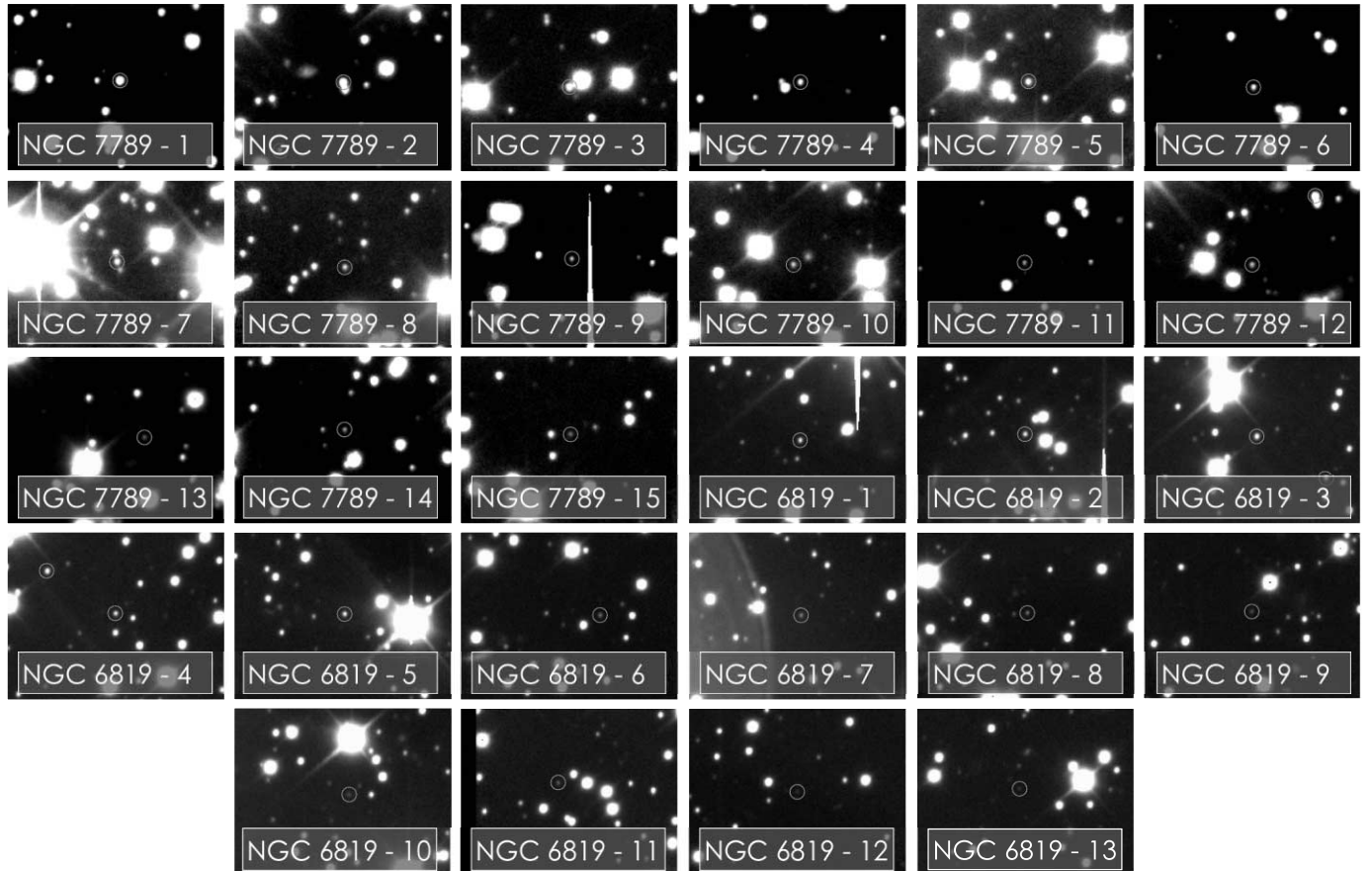


FIG. 5.—Images of each of our white dwarf candidates, shown from the V -band CFHT data. Each star is displayed in a small window that extends approximately $1'$ in the east-west direction (*east is to the left*) and $35''$ in the north-south direction (*north is up*). By design, most of the white dwarf candidates are well-isolated, sharp sources. [See the electronic edition of the Journal for a color version of this figure.]

TABLE 2
PHOTOMETRIC PROPERTIES OF WHITE DWARF CANDIDATES

ID	$\alpha_{\text{J}2000.0}$	$\delta_{\text{J}2000.0}$	V	$B-V$
NGC 7789-1	23 56 32.51	56 35 21.6	21.00 \pm 0.01	-0.04
NGC 7789-2	23 56 44.25	56 38 09.7	21.28 \pm 0.01	0.29
NGC 7789-3	23 56 36.62	56 40 23.5	22.13 \pm 0.02	0.01
NGC 7789-4	23 56 43.03	56 35 56.2	22.37 \pm 0.02	0.16
NGC 7789-5	23 56 49.06	56 40 13.2	22.49 \pm 0.01	0.04
NGC 7789-6	23 56 31.94	56 36 59.2	22.66 \pm 0.02	0.17
NGC 7789-7	23 56 51.93	56 38 21.3	22.62 \pm 0.01	0.19
NGC 7789-8	23 56 57.22	56 40 01.1	23.15 \pm 0.02	0.15
NGC 7789-9	23 56 42.42	56 32 48.4	23.09 \pm 0.02	0.35
NGC 7789-10	23 56 44.91	56 39 58.8	23.23 \pm 0.02	0.24
NGC 7789-11	23 56 30.81	56 37 19.3	23.36 \pm 0.02	0.27
NGC 7789-12	23 56 45.84	56 37 55.1	23.26 \pm 0.02	0.35
NGC 7789-13	23 57 05.17	56 38 20.1	23.47 \pm 0.02	0.24
NGC 7789-14	23 56 37.78	56 39 08.4	23.55 \pm 0.02	0.21
NGC 7789-15	23 56 34.19	56 40 05.0	24.02 \pm 0.03	0.34
NGC 6819-1	19 41 25.70	40 02 53.9	21.73 \pm 0.01	0.05
NGC 6819-2	19 41 26.10	40 03 48.0	21.78 \pm 0.01	0.15
NGC 6819-3	19 41 48.06	40 03 17.0	21.90 \pm 0.01	-0.20
NGC 6819-4	19 41 46.80	40 03 08.2	21.87 \pm 0.01	0.09
NGC 6819-5	19 41 27.36	40 00 47.8	22.51 \pm 0.01	0.17
NGC 6819-6	19 41 19.96	40 02 56.1	22.94 \pm 0.02	0.07
NGC 6819-7	19 41 33.93	40 01 41.4	22.91 \pm 0.02	-0.02
NGC 6819-8	19 41 37.21	40 04 45.3	23.03 \pm 0.02	0.19
NGC 6819-9	19 41 25.20	40 01 30.2	23.45 \pm 0.03	0.33
NGC 6819-10	19 41 32.13	40 01 07.8	23.86 \pm 0.04	0.39
NGC 6819-11	19 41 53.95	40 04 05.7	24.05 \pm 0.05	0.27
NGC 6819-12	19 41 32.76	40 04 39.9	24.10 \pm 0.06	0.33
NGC 6819-13	19 41 32.18	40 05 59.7	24.20 \pm 0.06	0.27

NOTE.—Units of right ascension are hours, minutes, and seconds, and units of declination are degrees, arcminutes, and arcseconds.

the temperature or mass of the star from the helium lines. Kalirai et al. (2005a) proposed that the absence of DBs in open clusters may be related to the fact that this population of white dwarfs is more massive than the field population (where we typically find 20%–25% DBs). This results from the targeting of younger clusters in previous studies (more massive progenitor stars) that have only produced massive white dwarfs. Such hot, high-mass white dwarfs may not develop large enough helium convection zones to allow helium to be brought to the surface and turn a hydrogen-rich white dwarf into a helium-rich one. Kalirai et al. predicted that an increasing number of DB white dwarfs should be seen as observations begin to probe older clusters, such as NGC 6819 and NGC 7789.

The second object, NGC 6819-8, shows very broad H β and H γ absorption lines but an absence of higher order Balmer lines. Although the spectral quality is not high enough to absolutely rule out the presence of weak higher order lines, this signature may suggest that the white dwarf is quite massive (see § 6 for more information). Furthermore, there is evidence for Zeeman splitting of the lines (see two panels on the right), and therefore this object is likely a magnetic white dwarf (see, e.g., Liebert et al. 2003). Again, the quality of the spectrum is too poor to estimate the magnetic field or the stellar mass, and therefore it would be useful to obtain higher S/N spectral observations of this star. In addition, a reduction of the red side spectrum from LRIS may shed further light on this interesting object. Given the poor quality, we also speculate whether the observed splitting may actually represent emission in the core of the Balmer absorption lines, in which case this object may be a binary system in which

the primary is accreting material from the secondary star. If the primary is massive enough, such a system could be a potential Type Ia supernova progenitor. Hurley & Shara (2003) speculated that this cluster contains a large fraction of white dwarfs that once had binary companions, in addition to double degenerates, to reproduce the scatter along the cooling sequence. Note that the image of this star does not show any nearby companions (see Fig. 5).

Interestingly, object 7 in NGC 7789 shows both hydrogen and helium lines in its spectrum. These are again highlighted in the three panels showing different wavelength regions (Fig. 6, bottom right). At lower wavelengths, the first panel shows hydrogen lines at 3970 and 4101 Å (H ϵ and H δ) as well as helium lines at 3889 and 4026 Å. In the middle panels H γ is seen at 4340 Å as well as two helium lines at 4388 and 4471 Å. At longer wavelengths (third panel), H β is visible at 4861 Å as well as three more helium lines at 4713, 4922, and 5016 Å. This object(s) is therefore either a single DAB (mixed hydrogen and helium atmosphere) white dwarf, or a double degenerate (i.e., unresolved white dwarf–white dwarf binary) consisting of both a DA and a DB (helium atmosphere) star. Distinguishing between these two cases is very difficult without a much higher S/N spectrum of this target (see, e.g., Bergeron & Liebert 2002). Both cases are very interesting. DAB white dwarfs are rare and can shed light on diffusion processes in white dwarfs and help our understanding of the chemical evolution of these stars. If this object is in fact a binary, then the discovery of the DB white dwarf would in fact represent the fifth helium atmosphere white dwarf in an open cluster (see above for the other four such stars). The image of this source in Figure 5 does show two nearby neighbors; however, both of these other stars are red main-sequence dwarfs and therefore cannot account for the contaminant.

5.2. Lower Quality White Dwarf Spectra and Other Objects

In Figure 7 (top) we present spectra of fainter DA white dwarfs in our data set. These spectra are too noisy to yield accurate spectroscopic masses, and therefore we will ignore them in the subsequent analysis. However, it is reassuring that most of the faint blue targets in our spectroscopic study are in fact white dwarfs. First, this suggests that our target selection process in these rich clusters is efficient. As mentioned earlier, we also found a high success rate in our study of NGC 2099 (Kalirai et al. 2005b) and NGC 6791 (Kalirai et al. 2007). Second, these fainter white dwarfs can be followed up with future observations to improve the S/N of the spectra and therefore may eventually be important in placing constraints on the initial-final mass relation. The faintest white dwarfs may even represent descendants from more massive main-sequence stars and therefore allow a probe of the relation over a mass range, within a given cluster.

At the bottom of Figure 7 are spectra for five other objects along our line of sight. The most interesting case is NGC 6819-3, which exhibits the hydrogen Balmer series although the lines are not pressure broadened. This object is therefore either a field horizontal branch star, or a distant main-sequence dwarf of spectral type late A or early F. If the latter, the observed magnitude of the star ($V = 21.9$) implies a distance of ~ 80 kpc. Similarly, NGC 6819-11 and -5 appear to be background dwarfs of later spectral type. The other two spectra lack enough signal to accurately classify the objects. These could be cool DA white dwarfs, DB or DC white dwarfs, or other objects along the line of sight such as unresolved blue galaxies.

Overall, our spectra confirm that 22 of the 27 targets for which we extracted a spectrum are in fact white dwarf stars. We now proceed to analyze further the six white dwarfs in NGC 7789 and

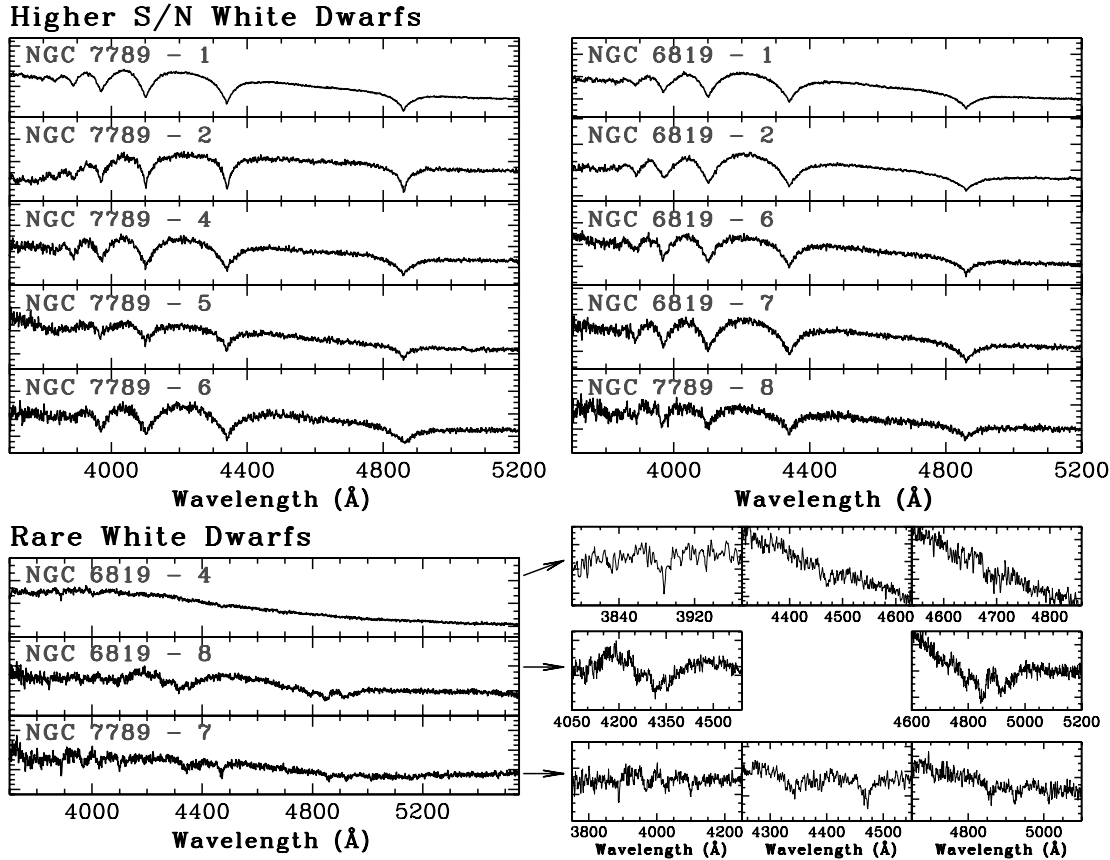


Fig. 6.—*Top:* Keck LRIS spectra for 10 stars with at least five well-characterized Balmer lines. Each of these stars can be fit to models to yield accurate temperatures and gravities (see § 6). *Bottom:* The spectra of three unique white dwarfs (*left*) and a closer look at their absorption lines (NGC 6819-4 and -8, and NGC 7789-7, *right*). NGC 6819-4 shows the presence of He lines at 3889, 4471, and 4713 Å, and is therefore a DB (helium atmosphere) white dwarf. NGC 6819-8 shows obvious signatures of very broad H β and H γ Balmer lines with possible Zeeman splitting, but no clear evidence of higher order Balmer lines. This star looks to be a massive, magnetic white dwarf. The spectrum of NGC 7789-7 shows both hydrogen and helium absorption lines. These objects are discussed further in § 5.1. [See the electronic edition of the Journal for a color version of this figure.]

four white dwarfs in NGC 6819 that show well-characterized Balmer lines (i.e., the top group in Fig. 6).

6. THE MASSES OF WHITE DWARFS IN NGC 7789 AND NGC 6819

Several techniques exist to measure the masses of white dwarfs, depending on what information is available. If the star is in a binary system, a dynamical mass estimate can be easily calculated from the orbit of the two stars. For example, the nearest white dwarf Sirius B was known to exist as early as 1841 from its dynamical influences on the optically brighter companion, Sirius A (Bessel 1844). The optical detection of the white dwarf did not occur until 1862 (by Alvan Clark), shortly after which the star was known to be a ~ 1 solar mass object from the period of the binary (~ 50 yr). For a white dwarf with a known radial velocity, the gravitational redshift method can also be used to measure the stellar mass (e.g., Adams 1925; Wegner 1989; Reid 1996). Given the large gravity, photons from the surface of the white dwarf will lose energy as they escape the potential of the star and therefore be redshifted (as first suggested by Michell 1784). To measure this effect, the H α Balmer line at 6563 Å is typically observed at intermediate resolution. Other methods to measure white dwarf masses are applicable to smaller subsets of stars only, e.g., pulsation mode analysis of very hot white dwarfs (Kawaler 1990) and fits to the mass-radius relation for stars with trigonometric parallaxes (Koester et al. 1979).

The most widely adopted technique for measuring the mass of a white dwarf involves fitting the Balmer lines of the spectrum to model atmospheres (Bergeron et al. 1992). The shapes of these line profiles depend sensitively on changes in the temperature (T_{eff}) and surface gravity ($\log g$) of the star. For example, as the atmospheric pressure in a white dwarf increases (e.g., due to a larger surface gravity), interactions between neighboring hydrogen atoms will lead to enhanced Stark broadening. For the lower order Balmer lines, this means the profiles will become broader (e.g., H β and H γ). However, the bluer Balmer lines are produced by electron transitions at higher energy levels, and therefore these lines will be the first to be destroyed by the increased perturbations on the atom (e.g., He ϵ , H 8 , H 9 , etc.). As an example of this, see Figure 3 in Bergeron et al. (1992). Therefore, using this technique to accurately define the T_{eff} and $\log g$ of a white dwarf requires the characterization of higher order Balmer lines in the stellar spectrum. For faint stars, this implies the need for a blue-sensitive spectrograph, as the wavelength of He is in the violet region, 3970 Å. With T_{eff} and $\log g$ constrained, the mass of the star can be obtained through a mass-radius relation.

A significant sample of white dwarfs has been observed using at least two of these techniques (including the spectroscopic Balmer line fitting technique) and therefore provide a means to independently check the accuracy of the method. Bergeron et al. (1995) analyze 35 such white dwarfs and find a reasonable agreement between spectroscopic mass determinations and gravitational

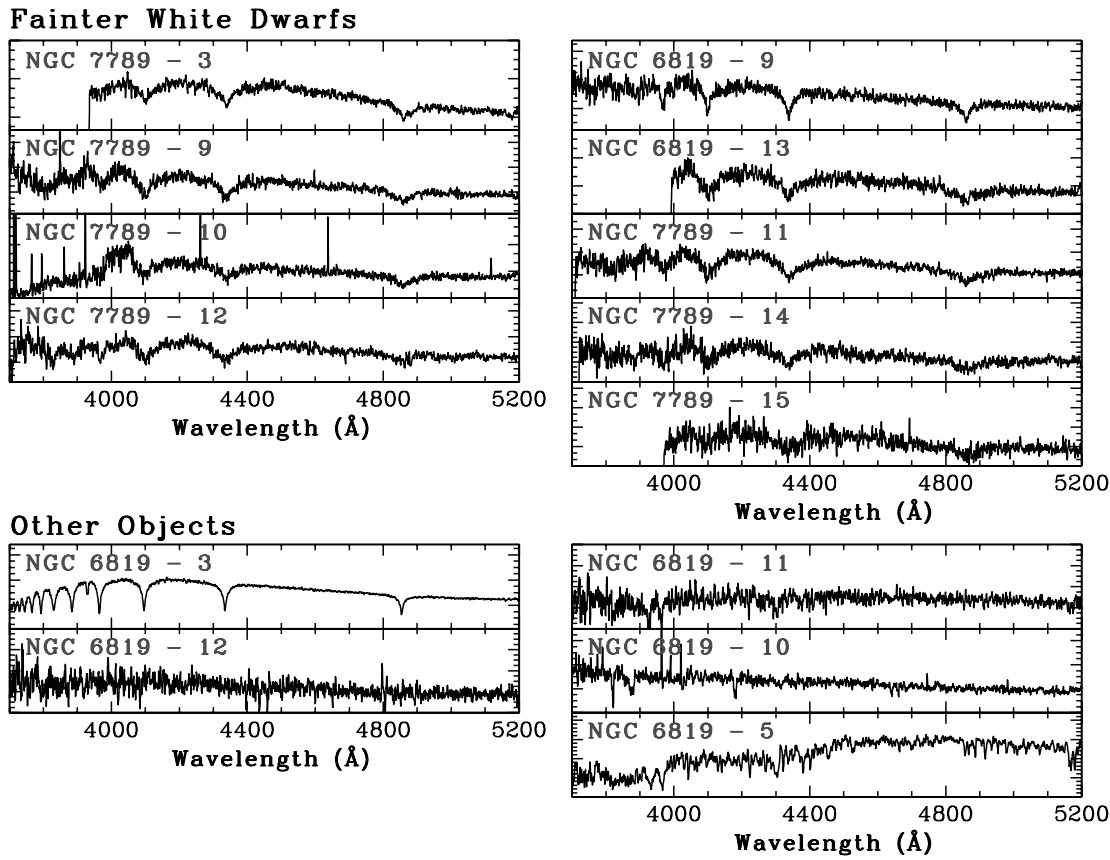


FIG. 7.—*Top:* Spectra for nine fainter white dwarfs in our data set. These spectra are too noisy to accurately characterize the shapes of the higher order Balmer lines, and therefore cannot be used to yield accurate temperatures and gravities for the stars. All of the stars can, however, be classified as DA white dwarfs. The spectra of NGC 7789-10 may even be contaminated by the galaxy seen near this star’s position in Fig. 5. The truncated spectral coverage of a few stars in this figure results from the locations of these objects in the field of view (close to the mask edge). *Bottom:* Spectra for five objects of likely non–white dwarf nature as discussed in § 5.2. [See the electronic edition of the Journal for a color version of this figure.]

redshifts for only those stars with $T_{\text{eff}} > 12,000$ K. For the cooler stars, the spectroscopic mass determinations are systematically larger than the gravitational redshifts by $\sim 0.1 M_{\odot}$. As pointed out by Bergeron et al. (1995) these measurements could be in error if convection has set in and polluted the atmospheres of these cool stars with helium (i.e., this would mimic a larger mass). A similar study by Reid (1996) based on HIRES spectra of 53 white dwarfs also found good agreement between these two methods for white dwarfs with $T_{\text{eff}} > 14,000$ K (see also Claver et al. 2001). Finally, a recent study with the *HST* Space Telescope Imaging Spectrograph has made it possible to calculate the mass of Sirius B using three independent techniques (Barstow et al. 2005). The mass of the white dwarf based on its orbit, gravitational redshift, and blue Balmer lines, all indicate that the star is 1 solar mass to within a few percent. As we show below, all but one of our white dwarfs have $T_{\text{eff}} > 13,000$ K, and therefore the spectroscopic mass measurements are not affected by any of these possible systematic errors.

The fitting technique to derive T_{eff} and $\log g$ is described in Bergeron et al. (1992). We convolved the models with a Gaussian profile with FWHM = 4 Å to match the resolution of our spectra. All of the available Balmer lines of each star are fit simultaneously, and the best-fit solution is converged on by minimizing χ^2 using the nonlinear least-squares method of Levenberg-Marquardt (Press et al. 1986). In this fit, the estimation of the continuum near each Balmer line is performed using the upgraded method described in Liebert et al. (2005a). The atmosphere models cover a $\log g$ range from 6.5 to 9.0 and a T_{eff} range from 1500 to 100,000 K.

The best solutions for the 10 white dwarfs in NGC 7789 and NGC 6819 are illustrated in Figure 8. For each star, we present the observed Balmer lines one on top of another, with H β at the bottom and subsequent higher order lines at the top (up to H9 at 3835 Å). The best-fit model solution for each is shown as a smooth profile (*solid curve*). The fits are excellent in all cases except for NGC 6819-2, in which the lower order Balmer lines are not reproduced as well as the higher order lines. If we ignore the higher order lines of this star and refit only H β , H γ , and H δ , the quality of the fit does not improve and the derived parameters of the star remain essentially unchanged. As we show below in § 7.1, this star is *not* a cluster member and therefore does not enter into our analysis of the initial-final mass relation.

White dwarf masses (M_{final}) are calculated for each star by interpolating the T_{eff} and $\log g$ within the updated evolutionary models of Fontaine et al. (2001) for a 50/50 carbon-oxygen core mix. The models adopt thick hydrogen layers [$q(\text{H}) = M_{\text{H}}/M = 10^{-4}$] and helium layers of $q(\text{He}) = 10^{-2}$. The models also provide white dwarf cooling ages (t_{cool}) for each star (i.e., the age of the star since shell helium burning finished on the asymptotic giant branch). We summarize the spectroscopic properties for these 12 white dwarfs in Table 3.

7. CALCULATING MAIN-SEQUENCE PROGENITOR LIFETIMES AND MASSES

Unlike for the field population of isolated white dwarfs, the environments of white dwarfs in star clusters can be used to shed light on the properties of their progenitors. As star clusters are

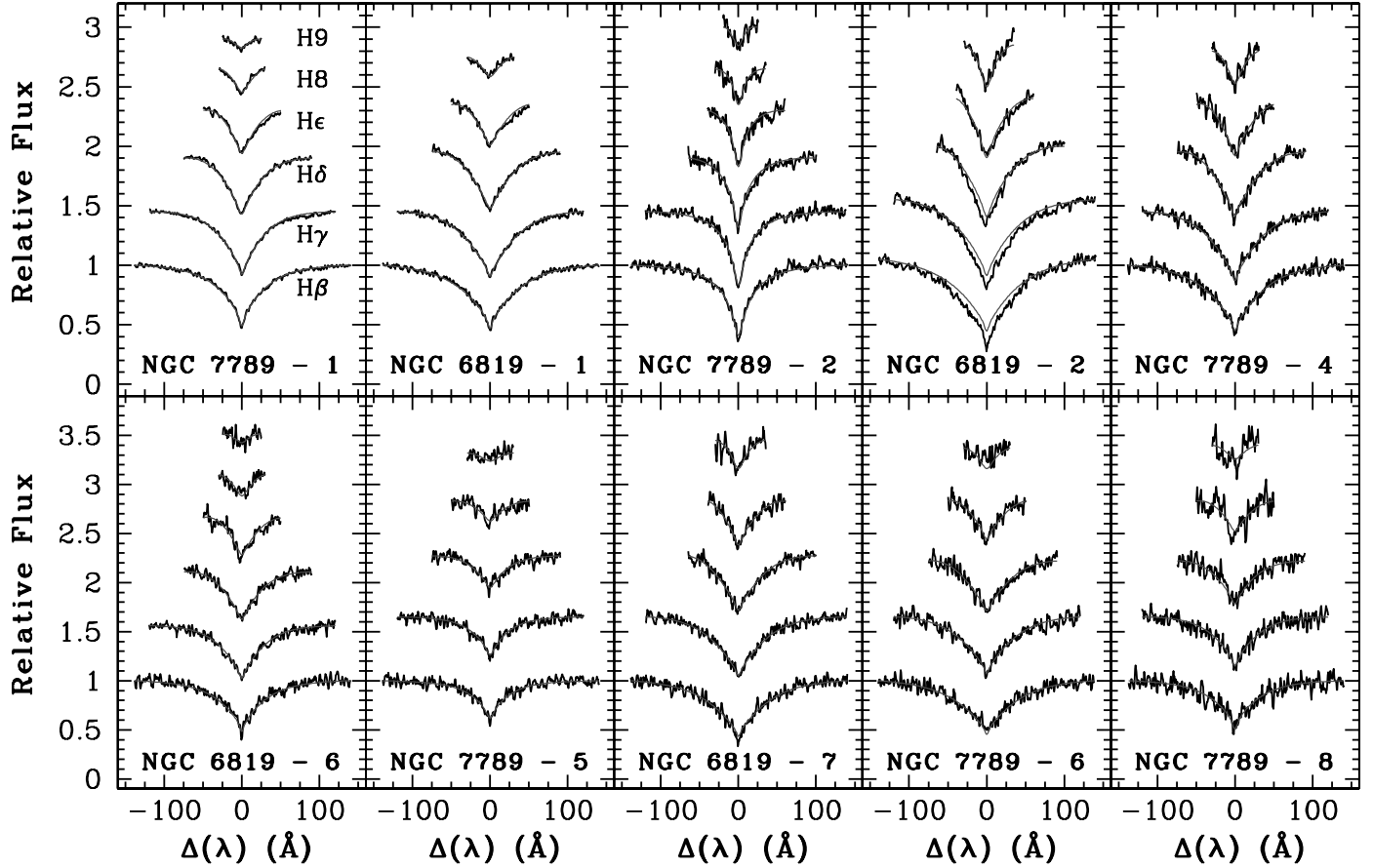


FIG. 8.—Best-fit hydrogen atmosphere model white dwarf spectrum (*solid curve*), shown for each of the 10 stars in Fig. 6 (*top*). Within each of the panels, the hydrogen Balmer lines for a single star are arranged with $H\beta$ at the bottom and successively higher order lines toward the top. The model shown represents the fit with the lowest χ^2 to all lines simultaneously. As discussed in § 6, these fits provide accurate measurements of both T_{eff} and $\log g$ (and therefore the stellar mass) for each white dwarf (see Table 3). [See the electronic edition of the Journal for a color version of this figure.]

coeval, the main-sequence turnoff ages of NGC 7789 and NGC 6819 measured in § 3.1 also represent the *total* lifetime of their member white dwarfs (i.e., the main-sequence lifetime plus the timescales for evolutionary stages beyond core hydrogen burning). Therefore, by subtracting the white dwarf cooling age from the cluster age, we can calculate the lifetime of the progenitor star that made the white dwarf up to the tip of the asymptotic giant

branch. For clusters as old as NGC 7789 and NGC 6819, this latter age (t_{ms}) is dominated by the main-sequence lifetime of the star, since the post-main-sequence evolutionary phases are short lived.

7.1. Cluster Membership

The assumption in the above calculation is that the spectroscopically confirmed white dwarfs in this study are in fact

TABLE 3
DERIVED PARAMETERS OF WHITE DWARFS

ID (1)	V_{obs} (2)	$V_{\text{theory}}^{\text{a}}$ (3)	T_{eff} (K) (4)	$\log g$ (5)	M_{final} (M_{\odot}) (6)	t_{cool} (Myr) (7)	t_{ms} (Myr) (8)	M_{initial} (M_{\odot}) (9)	Member? (10)
NGC 7789-1	21.00 ± 0.01	22.91 ± 0.11	$21,900 \pm 100$	7.89 ± 0.01	0.56 ± 0.01	35 ± 1	No
NGC 7789-2	21.28 ± 0.01	25.24 ± 0.14	$9,700 \pm 50$	8.31 ± 0.03	0.80 ± 0.02	1040 ± 64	No
NGC 7789-3 ^c	22.37 ± 0.02	23.40 ± 0.13	$16,900 \pm 200$	7.90 ± 0.03	0.56 ± 0.02	115 ± 8	1285 ± 140	$2.08^{+0.08}_{-0.08}$?
NGC 7789-5	22.49 ± 0.01	22.21 ± 0.18	$31,200 \pm 200$	7.90 ± 0.05	0.60 ± 0.03	8 ± 1	1392 ± 140	$2.02^{+0.07}_{-0.14}$	Yes
NGC 7789-6 ^c	22.66 ± 0.02	23.67 ± 0.18	$17,600 \pm 300$	8.15 ± 0.06	0.72 ± 0.03	160 ± 16	1240 ± 141	$2.10^{+0.09}_{-0.09}$?
NGC 7789-8	23.15 ± 0.02	22.87 ± 0.21	$24,300 \pm 400$	8.00 ± 0.07	0.64 ± 0.04	29 ± 5	1371 ± 140	$2.02^{+0.09}_{-0.11}$	Yes
NGC 6819-1	21.73 ± 0.01	23.44 ± 0.13	$19,600 \pm 100$	8.25 ± 0.02	0.78 ± 0.01	130 ± 5	No
NGC 6819-2	21.78 ± 0.01	23.55 ± 0.24	$13,100 \pm 600$	7.82 ± 0.07	0.50 ± 0.04	261 ± 36	No
NGC 6819-6	22.94 ± 0.02	22.70 ± 0.16	$21,100 \pm 300$	7.83 ± 0.04	0.53 ± 0.02	39 ± 3	2461 ± 250	$1.60^{+0.06}_{-0.05}$	Yes
NGC 6819-7	22.91 ± 0.02	23.31 ± 0.16	$16,000 \pm 200$	7.91 ± 0.04	0.56 ± 0.02	143 ± 11	2357 ± 250	$1.62^{+0.07}_{-0.05}$	Yes

^a Theoretical luminosity from spectral fits (see § 7.1).

^b The errors in the main-sequence lifetimes include the uncertainties in the cooling ages and an assumed 10% uncertainty in the ages of the clusters (which would produce a systematic shift in the lifetimes for all stars in a cluster).

^c Possible cluster double degenerates.

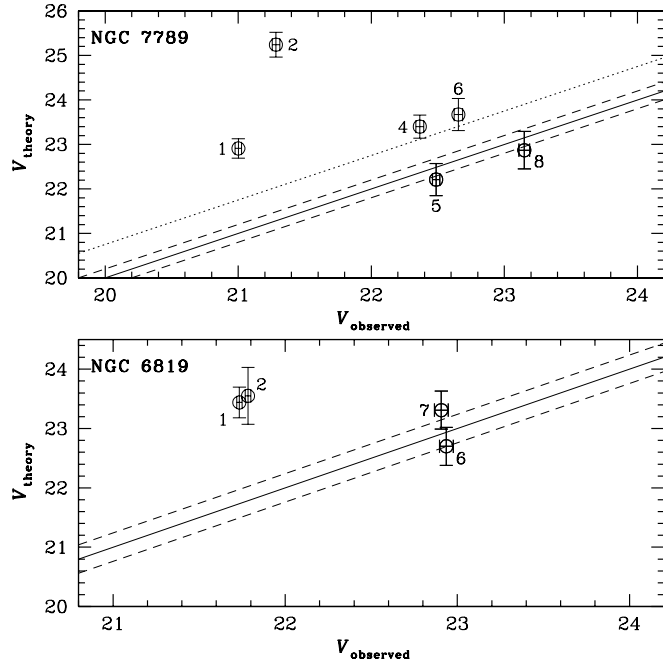


FIG. 9.—Comparison of the theoretical magnitude of the star (from fitting the Balmer lines) with the observed brightness, indicating that two of the white dwarfs in both NGC 7789 and NGC 6819 are single white dwarfs (*darker objects*) in these clusters (2σ error bars). An additional two objects in NGC 7789, objects 4 and 6, are consistent with being 0.75 mag overluminous, and therefore may represent unresolved double degenerate systems.

members of NGC 7789 and NGC 6819. As the volume probed increases with photometric depth, most of the field white dwarfs along these lines of sight will be found near the faint end of the data set. Depending on the distance and age of any field white dwarf, it could mimic itself as a faint blue cluster object.

To determine which of the stars are likely cluster white dwarfs, we use the white dwarf mass-radius relation to calculate a theoretical magnitude for each star. This magnitude is next compared to the observed brightness of the respective white dwarf by adopting the distance modulus of each cluster derived in § 3.1 [$(m - M)_V = 12.5 \pm 0.1$ for NGC 7789 and $(m - M)_V = 12.30 \pm 0.12$ for NGC 6819]. Figure 9 shows the results. The solid line represents the 1:1 relation, and the dashed lines are 2σ bounds based on the distance errors above. The uncertainties on the data points are also 2σ error bars. In NGC 7789, a group of four white dwarfs are found near the 1:1 relation, and two others are obvious outliers (objects 1 and 2). Based on this diagram, only objects 5 and 8 can be considered *isolated* cluster members (*darker points*). However, we note that both objects 4 and 6 are consistent with a 0.75 mag offset from the 1:1 relation (observed magnitude being too bright; *dotted line*). These stars are therefore overluminous by an amount consistent with an equal-mass binary nature (i.e., they could be unresolved double degenerates in the cluster), assuming they are not optical binaries. For NGC 6819, Figure 9 indicates that objects 6 and 7 are cluster members, whereas objects 1 and 2 are classified as nonmembers based on our parameter measurements.

For the four nonbinary cluster member stars and the two potential double degenerate systems, we measure the main-sequence plus post-main-sequence lifetimes (up to the tip of the asymptotic giant branch) by subtracting the derived white dwarf cooling ages from the cluster ages ($t = 1.4$ Gyr for NGC 7789 and $t = 2.5$ Gyr for NGC 6819; see § 3.1). These results, t_{ms} , are given in column (8) of Table 3. The main-sequence masses (M_{initial}) follow from the models of Hurley et al. (2000) and are listed in col-

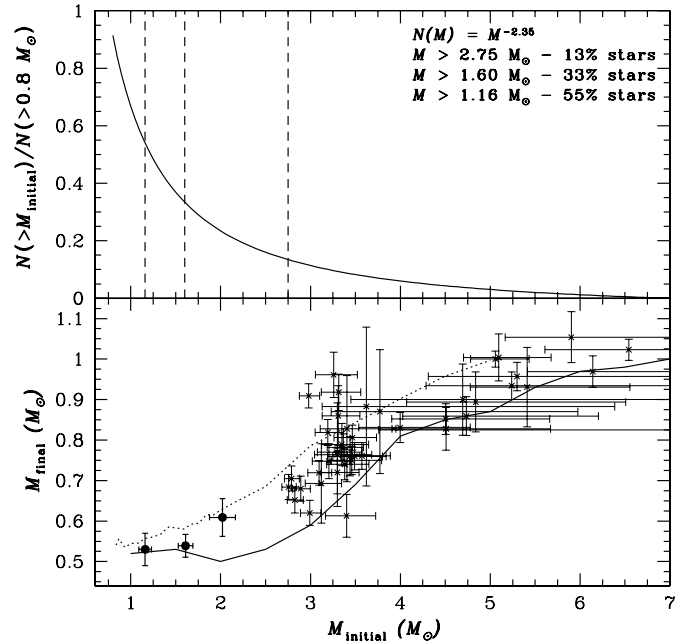


FIG. 10.—*Top:* For a Salpeter mass function: only 13% of all stars are formed with $M > 2.75 M_{\odot}$, whereas 55% have $M > 1.16 M_{\odot}$. *Bottom:* All previous constraints on the initial-final mass relation (crosses; see references in § 8.1) and weighted averages for the stars in this study (circles) from NGC 7789 ($M_{\text{initial}} = 2.03 M_{\odot}$) and NGC 6819 ($M_{\text{initial}} = 1.61 M_{\odot}$), as well as the masses of the single carbon-oxygen core white dwarf and progenitor in NGC 6791 ($M_{\text{initial}} = 1.16 M_{\odot}$). The uncertainties on these three points represent 2σ errors. The new data extend the initial-final mass relation to very low masses, and show that the observed trend at higher masses continues down to stars approximately the mass of the Sun. The two curves are the core mass at the first thermal pulse (solid) and the solar metallicity theoretical initial-final mass relation (dotted) from Marigo (2001).

umn (9) of Table 3. The errors in the main-sequence lifetimes include the uncertainties in the cooling ages and an assumed 10% uncertainty in the ages of the clusters. This latter uncertainty dominates the total error budget of the main-sequence lifetimes and would produce a systematic shift in these ages for all stars in a given cluster.

8. THE INITIAL-FINAL MASS RELATION

8.1. Constraining the Low-Mass End

We stressed earlier the importance of a well-constrained initial-final mass relation *over a wide mass range*. Star formation in the universe leads to an initial mass function that is generally steep (i.e., many more low-mass stars are produced as compared to high-mass stars; Salpeter 1955; Miller & Scalo 1979; Kroupa 2002). We illustrate a simple mass function with a Salpeter slope in Figure 10 (*top*), for 1000 stars over a mass range of $0.8 - 7 M_{\odot}$. These limits have been chosen as they range from the lowest mass stars that could have formed white dwarfs over the age of the universe ($\sim 0.8 M_{\odot}$) to the most massive such stars ($\sim 7 M_{\odot}$). In the bottom panel, we illustrate the initial-final mass relation with all constraints over the past 30 years (*crosses*). This includes white dwarfs in the Hyades, Praesepe, and Pleiades (Claver et al. 2001; Dobbie et al. 2004, 2006), NGC 3532 (Koester & Reimers 1993), NGC 2516 (Koester & Reimers 1996), NGC 2168 (Williams et al. 2004), NGC 2099 (Kalirai et al. 2005b), NGC 6633 (Williams & Bolte 2007), and Sirius B (Liebert et al. 2005b). Initial and final masses are taken from Table 1 in Ferrario et al. (2005). The only stars ignored in this analysis are four white dwarfs in young clusters with masses $< 0.55 M_{\odot}$ that likely represent field contamination

(e.g., see Kalirai et al. [2005b] for NGC 2099) and two stars with >90% uncertainties in their initial masses (star 3532-10 in NGC 3532 and 2099-WD16 in NGC 2099). Over the region where information is available ($M_{\text{initial}} > 2.75 M_{\odot}$; *right dashed line*), the relation shows a trend indicating that more massive main-sequence stars produce more massive white dwarfs. Integrating the Salpeter mass function above this limit, we find that *only* 13% of all stars are born with masses this large over the $0.8-7 M_{\odot}$ mass range. Therefore, the present initial-final mass relation cannot be directly used to infer progenitor properties for almost all white dwarfs in the Galactic disk and halo.

The $2.75 M_{\odot}$ lower initial mass limit on the relation results purely from an observational limitation. A low-mass ($0.6 M_{\odot}$), bright white dwarf has $M_V \sim 11$ at an age of ~ 100 Myr. At a distance of 1.5 kpc, this translates to an observed magnitude of $V \sim 22$. A more massive white dwarf at this age will be even fainter in the V band. As discussed above, measuring a spectroscopic mass for a white dwarf requires the accurate characterization of higher order Balmer lines with $\lambda < 4000 \text{ \AA}$. Achieving this for a $V = 22$ star obviously requires both a large telescope and a blue-sensitive spectrograph. Since very few rich (e.g., $>1000 M_{\odot}$), old star clusters are located within 1.5 kpc of the Sun (M67 is the only one), the targeted systems have typically been poorly populated, nearby, younger systems (such as the Hyades, Pleiades, and Praesepe). These clusters have ages of a few hundred megayears and therefore are not old enough to have allowed the evolution of lower mass stars off the main sequence.

The masses of white dwarfs in systems such as NGC 7789 and NGC 6819 present us the opportunity to extend the mass range over which the initial-final mass relation has been studied. The younger of our two clusters, NGC 7789, has an age of 1.4 Gyr. The main-sequence turnoff of this system is therefore $2.0 M_{\odot}$ (VandenBerg et al. 2006), and most of the cluster white dwarfs will have evolved from stars just above this mass (again, due to the slope of the mass function). The age of NGC 6819 is 2.5 Gyr, and therefore the present-day turnoff mass is $1.6 M_{\odot}$. The progenitor masses for the confirmed white dwarfs in each cluster are indeed very similar to one another, and just above the turnoff masses (see M_{initial} in Table 3).

We can also add data from the very old cluster NGC 6791 to the initial-final mass relation. At an age of 8.5 Gyr, this system represents one of the oldest open star clusters and has a main-sequence turnoff mass of $\sim 1.1 M_{\odot}$. Kalirai et al. (2007) present evidence that a significant population of white dwarfs in this cluster resulted from progenitors that expelled enough mass on the red giant branch to avoid the helium flash, and therefore the white dwarfs have helium cores rather than carbon-oxygen cores. This is believed to be a result of the high metallicity of the system, $[\text{Fe}/\text{H}] = +0.4$. The mean mass of the nine cluster white dwarfs targeted in that study is $\langle M \rangle = 0.43 M_{\odot}$. The threshold at which a helium core white dwarf is produced at NGC 6791's metallicity is $0.45-0.47 M_{\odot}$, and therefore to be conservative, we consider only the single confirmed cluster member with a mass $>0.50 M_{\odot}$ (definite carbon-oxygen core white dwarf). This object, NGC 6791 WD 7, has $M_{\text{initial}} = 1.16^{+0.04}_{-0.03}$ and $M_{\text{final}} = 0.53 \pm 0.02 M_{\odot}$ (see Kalirai et al. [2007] for the spectral fits). The initial mass for this star has been calculated using the same Hurley et al. (2000) models as for NGC 7789 and NGC 6819, for $Z = 0.035$ (the highest metallicity available in these models). We note that this data point may still represent a lower limit (i.e., the final mass), since the progenitor star of the carbon-oxygen core white dwarf also likely suffered from enhanced mass loss. The weighted mean progenitor mass and white dwarf mass for the two stars in NGC

7789, the two stars in NGC 6819, and the masses of the single object in NGC 6791 are

NGC 7789: $M_{\text{initial}} = 2.02 \pm 0.07 M_{\odot}$, $M_{\text{final}} = 0.61 \pm 0.02 M_{\odot}$,
 NGC 6819: $M_{\text{initial}} = 1.61 \pm 0.04 M_{\odot}$, $M_{\text{final}} = 0.54 \pm 0.01 M_{\odot}$,
 NGC 6791: $M_{\text{initial}} = 1.16 \pm 0.04 M_{\odot}$, $M_{\text{final}} = 0.53 \pm 0.02 M_{\odot}$.

We illustrate these new points as circles on the initial-final mass relation in Figure 10 (*bottom*). The calculated initial progenitor masses (for bright white dwarfs) in these much older clusters are all essentially the same, as the cooling ages are a very small fraction of the cluster ages. We have therefore plotted one data point for each cluster, which for the two clusters with multiple white dwarfs, represents the weighted mean of the system's progenitor and white dwarf masses. Also shown is the 2σ error in each quantity for all three clusters (see § 8.4 for more information on this). As expected, these new data points provide constraints on the low-mass end of the relation. They clearly indicate that the observed trend at higher masses (suggesting more massive main-sequence stars produce more massive white dwarfs) continues down to stars that are roughly 1 solar mass.

8.2. Theoretical Estimates of Stellar Mass Loss

Most of the mass loss that a star suffers through its evolution occurs during very short lived post-main-sequence evolutionary phases such as the red giant branch, asymptotic giant branch, and planetary nebula phases (e.g., see Reimers 1975). In fact, it is the mass loss that is responsible for concluding fusion processes in the star and hence its rise in luminosity on the asymptotic giant branch. In principle, the masses of the stellar cores during these last phases of stellar evolution can be determined directly from modeling these evolutionary stages. An ideal model would then take an initial star of a certain mass ($M \lesssim 8 M_{\odot}$) and propagate it through all phases of stellar evolution to yield a remnant white dwarf with a particular mass. In practice, this has been very difficult because the mass-loss mechanisms (e.g., helium flash and thermal pulses on the asymptotic giant branch) are not theoretically understood well enough (Weidemann 2000; see also Habing [1996] for a review). Direct observational constraints are rare given the very short lifetimes of stars on the asymptotic giant branch and planetary nebula phases ($\sim 10^5$ yr), and heavy obscuration of sources by dusty shells.

Recently, a few attempts have been made to calculate the rate of mass loss in asymptotic giant branch stars after factoring in parameters such as metallicity (e.g., Marigo 2001). We first present the mass of the stellar core at the first thermal pulse from one such calculation as a solid line in the bottom panel of Figure 10 (Girardi et al. 2000). As expected, this curve falls below the bulk of the data points, as it represents an evolutionary point before the core of the star has had a chance to grow during the thermal pulses. Note that the mass of the core is roughly constant for masses below $2 M_{\odot}$. From this initial point, Marigo (2001) performs synthetic calculations of the subsequent thermally pulsating phases of the asymptotic giant branch until the star has completely ejected its envelope (see details in her paper). This can therefore be used to predict both the total mass loss and specific chemical yields as a function of initial mass and metallicity. For solar metallicity, the theoretical initial-final mass relation from this work is shown as the dotted line in Figure 10 (*bottom*). For $M_{\text{initial}} > 4 M_{\odot}$, this curve is systematically higher than the observed data, predicting final remnant masses that are too large

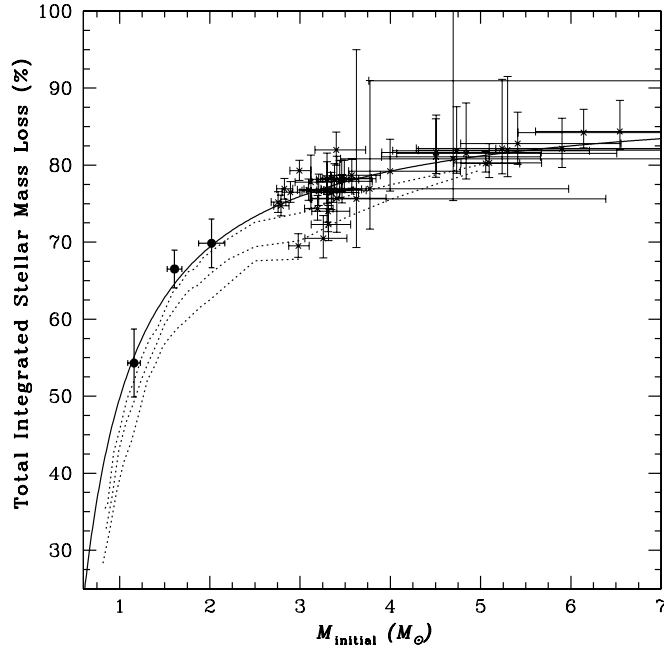


FIG. 11.—Total integrated mass loss, found to decrease as the initial mass of the star decreases. The new data points from this study, with 2σ error bars, are shown as circles. The dotted lines are theoretical calculations from Marigo (2001) for solar metallicity (top), $Z = 0.008$ (middle), and $Z = 0.004$ (bottom). The solid curve is the best-fit linear least-squares parameterization of the initial-final mass relation from this work (see § 8.4).

by up to $0.1 M_\odot$. A test of this relation at the low-mass end (i.e., the new data points with $M \lesssim 2 M_\odot$) also finds final masses that are larger than our observations; however, the differences are very small. Part of this difference may even be expected in the case of NGC 6791, given the 2.5 times higher metallicity of this cluster as compared to the solar metallicity theoretical relation (see earlier discussion).

In Figure 11 we present a different view of the initial-final mass relation to highlight the desired output from this work. The vertical axis now shows the total integrated mass loss through stellar evolution. For the most massive main-sequence stars that will form white dwarfs, this yield is about $\sim 85\%$ (e.g., the progenitor of white dwarf LB 1497 in the Pleiades). A slightly less massive star such as the progenitor of Sirius B ($5.06 M_\odot$; Liebert et al. 2005b) has lost 80% of its mass. The mass loss smoothly decreases with stellar mass down to $\sim 75\%$ for intermediate-mass stars, $3 M_\odot < M_{\text{initial}} < 4 M_\odot$. Our new data points suggest a more rapid decline for stars with $M \lesssim 2 M_\odot$. At this mass, stars will lose $\sim 70\%$ of their total mass; however, this decreases down to just $\sim 55\%$ for stars approximately the mass of the Sun. The theoretical calculation for solar metallicity discussed above is shown as the uppermost dotted curve (Marigo 2001).

8.3. The Scatter in the Relation

Several authors have commented on the observed scatter in the initial-final mass relation (e.g., Ferrario et al. 2005). The present data set is very heterogeneous. The points on Figure 10 are derived from white dwarf observations in over 10 star clusters. The quality of these data and procedures used to fit the spectra vary from one investigation to another, and therefore small biases are likely to exist in the M_{final} values. A small amount of field contamination may even exist in the sample. In addition, the ages of the star clusters have been derived by different authors using different assumptions, techniques, and isochrones, and therefore the

calculations involved in determining M_{initial} will also have biases. Even within an individual study, the large error bars in M_{initial} for the massive stars in Figure 10 are a good example of the difficulty in assigning masses to main-sequence lifetimes (see Ferrario et al. [2005] for a version of the relation with stars from individual clusters color coded). A small shift in the age of a cluster from 80 to 100 Myr results in a $>0.5 M_\odot$ systematic change in the inferred main-sequence mass at the turnoff. Measuring the ages of clusters to this precision is very difficult for such young systems where the morphology of the turnoff is essentially vertical on an optical CMD. This is of course not a large concern in the study of older clusters, since the turnoff can be well defined and the turnoff mass does not sensitively depend on the age.

Although characterizing the errors resulting from these uncertainties and heterogeneities is difficult, it is important to distinguish these biases from *intrinsic* scatter that may result from fundamental properties of stellar evolution. One way to minimize the systematic effects is to limit the study of a particular question to just the constraints from a few star clusters with many white dwarfs. For example, the Hyades (Perryman et al. 1998) is of similar age to NGC 2099 (Kalirai et al. 2001a, 2005b), yet its chemical abundance is enriched by a factor of 2 ($Z_{\text{Hyades}} = 0.025$ and $Z_{\text{NGC 2099}} = 0.013$). Models of stellar evolution predict that stars of higher metallicity will lose mass in post-main-sequence phases more efficiently than stars of lower metallicity (e.g., Marigo 2001). This is illustrated in Figure 11. As we said above, the dotted line at the top represents the theoretical estimates for mass loss in solar metallicity stars. The two dotted lines underneath are the same relation for more metal-poor stars, $Z = 0.008$ and $Z = 0.004$ (Marigo 2001). Fortunately, both the Hyades and NGC 2099 harbor significant white dwarf populations that have been studied spectroscopically. Kalirai et al. (2005b) showed that the mean mass of the NGC 2099 white dwarf population appears to be more massive (by $\sim 10\%$) than the Hyades stars, qualitatively consistent with the expectations from stellar evolution (this is a 2σ effect in the mean mass of the populations). As already discussed, a convincing example of the efficiency of mass loss on metallicity is presented in Kalirai et al. (2007). These cases highlight how the different properties of stars may play a role in contributing to the observed scatter on the initial-final mass relation.

Other properties of stars may also be important in understanding the scatter in the relation, such as rotation, binary evolution, and magnetic fields (see Weidemann 2000). Unfortunately, the quality of the present data does not permit a study of these effects. The mass-loss mechanisms may themselves be stochastic to some degree. For example, Reid (1996) measured masses of white dwarfs in the Praesepe using gravitational redshifts and found a large dispersion in the remnant mass distribution (0.6 – $0.9 M_\odot$). An estimate of the initial masses of these stars suggests that they were all produced from stars of about the same mass. This would then suggest that there is no singular initial-final mass relation. However, Claver et al. (2001) reconcile this picture by suggesting that one of the outlier stars in the M_{initial} versus M_{final} plane of the Praesepe sample (LB 5893) may have formed from close binary evolution. A better understanding of these types of effects will require a larger data set, as we discuss below.

8.4. Semiempirical Relations and Parameterization

Deriving a functional form of the initial-final mass relation from the available data is problematic for several reasons. First, for the reasons discussed above, such a parameterization may be meaningless given the uncertain degree to which second-order properties of stars may effect their mass loss. Second, the relation is only constrained over a fraction of the total mass range that is

of interest. Prior to this work, the low-mass end of the relation was completely devoid of any observations of individual white dwarfs with direct mass measurements. The high-mass end continues to be sparsely populated, the degree to which depends on the maximum mass of a star that will form a white dwarf (the current highest mass point observed is at $M_{\text{initial}} = 6.5 M_{\odot}$; Ferrario et al. 2005).

Weidemann (2000) calculates a semiempirical initial-final mass relation based on the available data at the time. At the low-mass end, his relation is constrained by an anchor point at $M_{\text{initial}} = 1 M_{\odot}$, $M_{\text{final}} = 0.55 M_{\odot}$, which is in good agreement with the mass of the core at the first thermal pulse. The general shape of the relation and possible slope changes are discussed in detail. Interestingly, at the low-mass end the data indicate that the relation flattens off as the initial-mass scale continues down to $0.8 M_{\odot}$, similar to the core-radius relation shown in Figure 10. The NGC 6819 data point at $M_{\text{initial}} = 1.61 M_{\odot}$, $M_{\text{final}} = 0.54 M_{\odot}$ is already within a few hundredths of a solar mass of the core mass ($\sim 0.5 M_{\odot}$ depending on Z ; see core mass relation in Fig. 10; see also Pietrinferni et al. 2004). The final mass of the carbon-oxygen core white dwarf in NGC 6791 is slightly lower than this, and equal to the expected mass of white dwarfs in globular clusters ($M_{\text{final}} = 0.53 M_{\odot}$; Renzini & Fusi Pecci 1988; Renzini et al. 1996; Moehler et al. 2004) with present-day turnoffs of $M_{\text{initial}} = 0.8 M_{\odot}$. This flattening of the relation suggests an exponential-like behavior at low masses. Unfortunately, such a parameterization would not fit the high-mass end of the relation very well, since those data also appear to show a flattening off. As noted by Weidemann (2000) the higher mass stars may in fact form white dwarfs that are structurally different, in that they have neon/oxygen cores instead of carbon-oxygen cores. Reproducing the relation for stars with masses greater than $\sim 4.5 M_{\odot}$ can be accomplished with a log function; however, this would grossly mismatch the masses of the white dwarfs at the low-mass end.

Lacking a satisfactory functional form of the type discussed above over the entire mass range in Figure 10, we resort to a simple linear fit as performed in the synthesis given by Ferrario et al. (2005). These authors took advantage of several recent studies (see earlier references) that have now more than doubled the amount of data as compared to the Weidemann (2000) study (all for $M_{\text{initial}} > 2.75 M_{\odot}$). However, unlike that study, we will use no anchor point to fix the relation at the low-mass end, which is otherwise needed to avoid a meaningless slope given the large scatter at intermediate masses (Ferrario et al. introduced a point at $M_{\text{initial}} = 1.1 M_{\odot}$, $M_{\text{final}} = 0.55 M_{\odot}$). We also follow the approach introduced by Williams (2007) and bin the relation so that each star cluster is represented as a single point (including Sirius B). This has a few advantages. First, our fit will not be overinfluenced by the region of the relation with the most data points. Second, the standard deviation in the distribution of masses of white dwarfs within a given cluster is a random error on the relation when comparing different clusters (Williams 2007). When plotting individual data points, an error in the age of a cluster will lead to a systematic offset of all points on the relation for that cluster. Third, our results will be less sensitive to any possible peculiar white dwarfs whose initial and final masses are measured accurately. The obvious disadvantage of the binned approach is that a given cluster is expected to have white dwarfs with a range of initial and final masses, and therefore we are throwing away this information.

The initial-final mass relation based on this binned method is shown in Figure 12. We note that the 2σ outlier at $M_{\text{initial}} = 5.06 M_{\odot}$ is Sirius B (Liebert et al. 2005b). The uncertainties in this plot are the standard deviations in the mean initial and final mass.

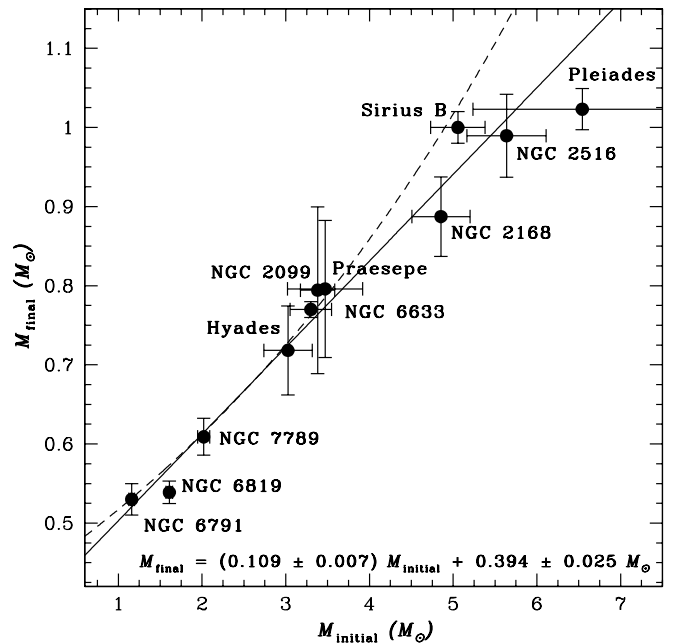


FIG. 12.—Initial-final mass relation, constructed by showing all of the stars from each cluster as a single data point, as labeled. The best-fit linear least-squares relation (solid curve) is indicated in the panel, and is found to provide an adequate fit to the data (reduced χ^2 per degree of freedom is $\chi^2 = 1.2$). The dashed curve shows the initial-final mass relation calculated by Hansen et al. (2007) to fit the white dwarf cooling sequence of the globular cluster NGC 6397 (see § 9).

The solid line represents our weighted linear least-squares best fit,

$$M_{\text{final}} = (0.109 \pm 0.007) M_{\text{initial}} + 0.394 \pm 0.025 M_{\odot}$$

Although an “S”-shaped relation with curvature would provide a better fit at both the lower and upper ends, we note that the reduced χ^2 per degree of freedom is $\chi^2 = 1.2$ in the linear fit, and therefore the data are well fit by this simple relation. If we also include a data point at $M_{\text{initial}} = 0.80 \pm 0.02 M_{\odot}$ and $M_{\text{final}} = 0.53 \pm 0.02 M_{\odot}$ to represent the best current globular cluster constraints (Renzini et al. 1996; Moehler et al. 2004), the relation flattens slightly to $M_{\text{final}} = (0.106 \pm 0.007) M_{\text{initial}} + 0.409 \pm 0.022 M_{\odot}$. In this case, the χ^2 of the fit is 1.3.

9. DISCUSSION AND CONCLUSIONS

A mapping of the initial mass of a hydrogen-burning star to its final remnant mass represents an extremely important relation in astrophysics. Over 99% of all stars will end their lives as white dwarfs and expel most of their mass into the interstellar medium. The initial-final mass relation allows us to directly integrate this mass loss in a stellar population assuming an initial mass function. Among the many uses of parameterizing this relation is a robust estimate for the ages of the Galactic disk and halo. For example, the shape of the white dwarf mass function in the Galactic disk is sharply peaked at $\sim 0.6 M_{\odot}$ (Liebert et al. 2005a; Kepler et al. 2007). The initial-final mass relation allows us to reconstruct the distribution of masses of the progenitor hydrogen-burning stars that formed this peak. This therefore provides an estimate of the age of the Galactic disk, which has now been measured to be $\sim 7\text{--}9$ Gyr (Winget et al. 1987; Wood 1992; Oswalt et al. 1996; Leggett et al. 1998; Hansen et al. 2002). For a Salpeter initial mass function, and an age of 8 Gyr for the Galactic disk, the shape of the predicted white dwarf mass distribution based on our initial-final mass relation is in excellent agreement with the observed

mass distribution (i.e., the peak location and spread; J. S. Kalirai et al. 2008, in preparation). Similarly, the ages of globular clusters in the Galactic halo have been measured to be ~ 12 Gyr by comparing the observed distribution of white dwarfs on the cluster CMDs to synthetic cooling sequences produced using an initial mass function and an initial-final mass relation (Hansen et al. 2004, 2007). The relation used most recently in the study of NGC 6397 by Hansen et al. (2007) is shown as a dashed line in Figure 12 and is found to be in good agreement with our new low-mass constraints (the disagreement at higher masses is not important, since all of the observed white dwarfs in NGC 6397 evolved from stars with $M < 2 M_{\odot}$).

The study of the white dwarf population in NGC 7789, NGC 6819, and NGC 6791 represents the first time that we have been able to reconstruct empirically this mapping for low-mass stars such as the Sun, and therefore eliminate the need for an indirect anchor point at low masses. Over half of the total number of stars that are produced in a Salpeter-type initial mass function now fall within a region of the initial-final mass relation that has some constraints. At high masses, the relation indicates that stars will lose 80%–85% of their mass through stellar evolution. However, for stars approximately as massive as the Sun, this number drops to $\sim 55\%$ of the initial stellar mass.

Despite these new data, the importance of the initial-final mass relation demands further observations. To better understand the intrinsic scatter, future observations should focus on older clusters with clearly defined white dwarf cooling sequences (such as NGC 7789). By pushing the magnitude limit fainter, more massive white dwarfs will be revealed that are likely descendants of more massive progenitors. In this way, multiple initial-final mass relations can be constructed over appreciable ranges from the studies of *single* star clusters whose properties (age, metallicity, binary fraction, etc.) have been measured carefully. Such studies are ideally suited for multiobject spectrographs since the white dwarf luminosity function increases as a function of magnitude, and therefore a large number of objects can be targeted in a single exposure. To truly push the envelope to even lower masses, globular clusters should be targeted as well. The nearest systems, such as M4 and NGC 6397, can be studied with 8–10 m tele-

scopes (e.g., see Moehler et al. 2004). In addition to providing constraints down to $\sim 0.8 M_{\odot}$, the environments of these systems are up to 100 times more metal-poor than most open clusters, and therefore metallicity trends can be reliably studied. At the opposite extreme, rich, young clusters can provide unique constraints and push the current high-mass limit further. This will not only constrain the upper mass limit to white dwarf production, but also simultaneously discover the lower mass limit to Type II supernovae. An extrapolation of the present relation to the Chandrasekhar mass suggests an initial mass of $\sim 9.5 M_{\odot}$; however, this is very uncertain given the lack of data in this regime. Finally, there is a paucity of data between $M_{\text{initial}} = 2$ and $2.75 M_{\odot}$ which can bridge our new measurements with the previous data. The absence of data points in this region of the relation results from a lack of nearby, rich star clusters with an age of ~ 1 Gyr. Fortunately, one such system exists, NGC 2420, and has been shown to possess a white dwarf population (von Hippel & Gilmore 2000) and therefore should be targeted in the near future.

We gratefully acknowledge P. Bergeron for providing us with his models and spectral fitting routines to measure the masses of white dwarfs. We also thank him and James Liebert for taking the time to discuss and help interpret the spectra of certain stars. We wish to thank Robert Eakin for assistance with processing of imaging data frames, and Don Vandenberg and Leo Girardi for their help with interpreting their models. Finally, we wish to extend our gratitude to an anonymous referee for taking the time to prepare a detailed report that has resulted in a much improved paper. J. S. K. is supported by NASA through Hubble Fellowship grant HF-01185.01-A, awarded by the Space Telescope Science Institute, which is operated by the Association of Universities for Research in Astronomy, Incorporated, under NASA contract NAS5-26555. Support for this work was also provided by grant HST-GO-10424 from NASA/STScI. The research of H. B. R. is supported by grants from the Natural Sciences and Engineering Research Council of Canada. He also thanks the Canada-US Fulbright Program for the award of a Fulbright Fellowship.

REFERENCES

- Adams, W. S. 1925, Proc. Natl. Acad. Sci., 11, 382 (reprint 1925, Observatory, 36, 2)
- Anthony-Twarog, B. J. 1981, ApJ, 245, 247
- . 1982, ApJ, 255, 245
- Barstow, M. A., Bond, H. E., Holberg, J. B., Burleigh, M. R., Hubeny, I., & Koester, D. 2005, MNRAS, 362, 1134
- Bergeron, P., & Liebert, P. 2002, ApJ, 566, 1091
- Bergeron, P., Liebert, J., & Fulbright, M. S. 1995, ApJ, 444, 810
- Bergeron, P., Saffer, R. A., & Liebert, J. 1992, ApJ, 394, 228
- Bertin, E., & Arnouts, S. 1996, A&AS, 117, 393
- Bessel, F. W. 1844, MNRAS, 6R, 136
- Bragaglia, A., et al. 2001, AJ, 121, 327
- Burbidge, E. M., & Sandage, A. 1958, ApJ, 128, 174
- Claver, C. F., Liebert, J., Bergeron, P., & Koester, D. 2001, ApJ, 563, 987
- de Bruijne, J. H. J., Hoogerwerf, R., & de Zeeuw, P. T. 2001, A&A, 367, 111
- Demarque, P., Woo, J.-H., Kim, Y.-C., & Yi, S. K. 2004, ApJS, 155, 667
- Dobbie, P. D., Pinfield, D. J., Napiwotzki, R., Hambly, N. C., Burleigh, M. R., Barstow, M. A., Jameson, R. F., & Hubeny, I. 2004, MNRAS, 355, L39
- Dobbie, P. D., et al. 2006, MNRAS, 369, 383
- Eisenstein, D. J., et al. 2006, ApJS, 167, 40
- Ferrario, L., Wickramasinghe, D., Liebert, J., & Williams, K. A. 2005, MNRAS, 361, 1131
- Fleming, T. A., Liebert, J., Bergeron, P., & Beauchamp, A. 1997, in Proc. 10th European Workshop on White Dwarfs, ed. J. Isern, M. Hernanz, & E. Gracia-Berro (Dordrecht: Kluwer), 91
- Fontaine, G., Brassard, P., & Bergeron, P. 2001, PASP, 113, 409
- Fusi-Pecchi, F., & Renzini, A. 1976, A&A, 46, 447
- Gim, M., Vandenberg, D. A., Stetson, P. B., Hesser, J. E., & Zurek, D. R. 1998, PASP, 110, 1318
- Girardi, L., Bertelli, G., Bressan, A., Chiosi, C., Groenewegen, M. A. T., Marigo, P., Salasnich, B., & Weiss, A. 2002, A&A, 391, 195
- Girardi, L., Bressan, A., Bertelli, G., & Chiosi, C. 2000, A&AS, 141, 371
- Habing, H. J. 1996, A&A Rev., 7, 97
- Hansen, B. M. S., et al. 2002, ApJ, 574, L155
- . 2004, ApJS, 155, 551
- . 2007, ApJ, 671, 380
- Harris, H. C., et al. 2006, AJ, 131, 571
- Hurley, J. R., Pols, O. R., & Tout, C. A. 2000, MNRAS, 315, 543
- Hurley, J. R., & Shara, M. M. 2003, ApJ, 589, 179
- Jeffries, R. D. 1997, MNRAS, 288, 585
- Kalirai, J. S., Bergeron, P., Hansen, B. M. S., Kelson, D. D., Reitzel, D. B., Rich, R. M., & Richer, H. B. 2007, ApJ, 671, 748
- Kalirai, J. S., Richer, H. B., Hansen, B. M. S., Reitzel, D., & Rich, R. M. 2005a, ApJ, 618, L129
- Kalirai, J. S., Richer, H. B., Reitzel, D., Hansen, B. M. S., Rich, R. M., Fahlman, G. G., Gibson, B. K., & von Hippel, T. 2005b, ApJ, 618, L123
- Kalirai, J. S., & Tosi, M. 2004, MNRAS, 351, 649
- Kalirai, J. S., Ventura, P., Richer, H. B., Fahlman, G. G., D'Antona, F., & Marconi, G. 2001a, AJ, 122, 3239
- Kalirai, J. S., et al. 2001b, AJ, 122, 257
- . 2001c, AJ, 122, 266
- Kawaler, S. D. 1990, in ASP Conf. Ser. 11, Confrontation Between Stellar Pulsations and Evolution, ed. C. Cacciari & G. Clemintini (San Francisco: ASP), 494
- Kelson, D. 2003, PASP, 115, 688
- Kelson, D. D., Illingworth, G. D., van Dokkum, P. G., & Franx, M. 2000, ApJ, 531, 159

- Kepler, S. O., Kleinman, S. J., Nitta, A., Koester, D., Castanheira, B. G., Giovannini, O., Costa, A. F. M., & Althaus, L. 2007, MNRAS, 375, 1315
- Koester, D., & Reimers, D. 1981, A&A, 99, L8
———. 1985, A&A, 153, 260
———. 1993, A&A, 275, 479
———. 1996, A&A, 313, 810
- Koester, D., Schulz, H., & Weidemann, V. 1979, A&A, 76, 262
- Kroupa, P. 2002, Science, 295, 82
- Landolt, A. U. 1992, AJ, 104, 340
- Leggett, S. K., Ruiz, M. T., & Bergeron, P. 1998, ApJ, 497, 294
- Liebert, J., Bergeron, P., & Holberg, J. B. 2003, AJ, 125, 348
———. 2005a, ApJS, 156, 47
- Liebert, J., Young, P. A., Arnett, D., Holberg, J. B., & Williams, K. A. 2005b, ApJ, 630, L69
- Marigo, P. 2001, A&A, 370, 194
- McCarthy, J. K., et al. 1998, Proc. SPIE, 3355, 81
- Michell, J. 1784, Philos. Trans. R. Soc. London, 74, 35
- Miller, G. E., & Scalo, J. M. 1979, ApJS, 41, 513
- Moehler, S., Koester, D., Zoccali, M., Ferraro, F. R., Heber, U., Napiwotzki, R., & Renzini, A. 2004, A&A, 420, 515
- Monelli, M., et al. 2005, ApJ, 621, L117
- Oke, J. B., et al. 1995, PASP, 107, 375
- Oswalt, T. D., Smith, J. A., Wood, M. A., & Hintzen, P. 1996, Nature, 382, 692
- Perryman, M. A. C., et al. 1998, A&A, 331, 81
- Pietrinferni, A., Cassisi, S., Salaris, M., & Castelli, F. 2004, ApJ, 612, 168
- Press, W. H., Flannery, B. P., & Teukolsky, S. A. 1986, Numerical Recipes: The Art of Scientific Computing (Cambridge: Cambridge Univ. Press)
- Reid, I. N. 1996, AJ, 111, 2000
- Reimers, D. 1975, Mem. Soc. R. Sci. Liège, 8, 369
- Reimers, D., & Koester, D. 1982, A&A, 116, 341
———. 1989, A&A, 218, 118
———. 1994, A&A, 285, 451
- Renzini, A., & Fusi Pecci, F. 1988, ARA&A, 26, 199
- Renzini, A., et al. 1996, ApJ, 465, L23
- Richer, H. B., et al. 2004, AJ, 127, 2771
———. 2006, Science, 313, 936
- Romanishin, W., & Angel, J. R. P. 1980, ApJ, 235, 992
- Salpeter, E. E. 1955, ApJ, 121, 161
- Somerville, R. S., & Primack, J. R. 1999, MNRAS, 310, 1087
- Stetson, P. B. 1994, PASP, 106, 250
- VandenBerg, D. A., Bergbusch, P. A., & Dowler, P. D. 2006, ApJS, 162, 375
- van den Bergh, S., & Tammann, G. A. 1991, ARA&A, 29, 363
- von Hippel, T., & Gilmore, G. 2000, AJ, 120, 1384
- Wegner, G. 1989, in IAU Colloq. 114, White Dwarfs, ed. G. Wegner (Berlin: Springer), 401
- Weidemann, V. 1977, A&A, 59, 411
———. 1987, A&A, 188, 74
———. 1997, in Advances in Stellar Evolution: Proceedings of the Workshop Stellar Ecology, ed. R. T. Rood & A. Renzini (Cambridge: Cambridge Univ. Press), 169
———. 2000, A&A, 363, 647
- Weidemann, V., & Koester, D. 1983, A&A, 121, 77
- Williams, K. A. 2007, in ASP Conf. Ser. 372, 15th European Workshop on White Dwarfs, ed. R. Napiwotzki & M. R. Burleigh (San Francisco: ASP), 85
- Williams, K. A., & Bolte, M. 2007, AJ, 133, 1490
- Williams, K. A., Bolte, M., & Koester, D. 2004, ApJ, 615, L49
- Williams, K. A., Liebert, J., Bolte, M., & Hanson, R. B. 2006, ApJ, 643, L127
- Winget, D. E., Hansen, C. J., Liebert, J., van Horn, H. M., Fontaine, G., Nather, R. E., Kepler, S. O., & Lamb, D. Q. 1987, ApJ, 315, L77
- Wood, M. A. 1992, ApJ, 386, 539
———. 1995, in White Dwarfs: Proceedings of the 9th European Workshop on White Dwarfs, ed. D. Koester & K. Werner (Berlin: Springer), 41
- Wu, Z.-Y., Zhou, X., Ma, J., Jiang, Z.-J., Chen, J.-S., & Wu, J.-H. 2007, AJ, 133, 2061